Title

HDA19-mediated deacetylation of histone H3.3 lysine 27 and 36 regulates plant sensitivity to salt stress

Authors

Florian Kotnik[1]†, Minoru Ueda[2,3]†, Akihiro Ito[4,5], Junko Ishida[2,3], Katsuyuki Sakai[6], Hiroshi Takagi[6], Julian Seidel[7], Takahiro Abe[2,8], Juergen Eirich[1], Shunji Takahashi[6], Dirk Schwarzer[7], Motoaki Seki[2,3,8,9]*. Iris Finkemeier[1]*

Affiliations

[1]Institute of Plant Biology and Biotechnology, University of Münster; Münster, 48149, Germany.
[2]Plant Genomic Network Research Team, RIKEN CSRS; Yokohama, 230-004, Japan.
[3]Plant Epigenome Regulation Laboratory, RIKEN CSRS; Wako, 351-0198, Japan.
[4]School of Life Sciences, Tokyo University of Pharmacy and Life Sciences; Hachioji, 192-0392, Japan
[5]Drug Discovery Seed Compounds Exploratory Unit, RIKEN CSRS; Wako, 351-0198, Japan.
[6]Natural Product Biosynthesis Research Unit, RIKEN; 351-0198, Japan.
[7]Interfaculty Institute of Biochemistry (IFIB), University of Tübingen, Tübingen, 72076, Germany.
[8]Kihara Institute for Biological Research, Yokohama City University; Yokohama, 244-0813, Japan
[9]Graduate School of Science and Engineering, Saitama University, Saitama, 338-8570, Japan

†These authors contributed equally to this work

*Corresponding author. Email: motoaki.seki@riken.jp (M.S.); finkemeier@uni-muenster.de (I.F.)

Abstract

Plants survive extreme environments through rapid chromatin reprogramming, while the epigenetic marks that confer this type of stress resilience remain poorly understood. Histone deacetylase HDA19 is a key epigenetic regulator in Arabidopsis, and *hda19* deficient mutants are tolerant to several abiotic stresses. Through acetylome profiling, we identified a non-canonical K27/K36 di-acetylation mark on histone H3.3 among nine H3 variants as a key substrate of HDA19. The epigenetic mark accumulation decreased and increased in wild-type plants and *hda19* mutants, whereas other known H3 marks were equally affected in response to salinity stress in both genotypes. Mimicking constitutive diacetylation of this H3K27/K36 mark led to the accumulation of stress resistance-mediating late embryogenesis abundant (LEA) proteins and induced salinity tolerance, similar to that observed in *hda19* mutants. The loss of function mutants of *lea7-1/lea29-1/rab18-1* abolished the salinity tolerance of *hda19*. Our findings show that histone H3.3 K27/K36 di-acetylation mediates LEA protein accumulation, enabling plants to withstand environmental stresses.

Teaser

A novel and non-canonical histone H3.3 di-acetylation mark is responsible for LEA protein mediated salt tolerance in *hda19*.

MAIN TEXT

Introduction

Abiotic stressors like salt stress pose significant threats to crop yields. Hence, the elucidation of the molecular mechanisms underlying plant stress responses is crucial for developing resilient crops. Histone deacetylase 19 (HDA19), also known as HDA1 or HD1, plays a key role in regulating gene expression during plant development and in response to stress (*1-3*). However, the mode of action of HDA19 in driving epigenetic regulatory machinery in response to stress remains unclear.

Within the nucleus of eukaryotic cells, core histone proteins (H2A, H2B, H3 and H4) wrap DNA into higher order structures called nucleosomes, enabling sophisticated regulation of nuclear gene expression and protecting DNA from physical damage. Multiple post-translational modifications (PTMs) can occur on the N-terminal tails of histones and play a crucial role in regulating chromatin structure and, consequently, gene expression. The most important histone PTMs include lysine acetylation, various other acylations, lysine and arginine methylation, lysine ubiquitination as well as serine and threonine phosphorylation. Based on the interplay of these modifications, which are essential for chromatin structure and gene activity regulation, a histone code theory was proposed (*4-6*). Previous studies have established a positive correlation between levels of lysine acetylation at N-terminal histone H3 sites and active gene expression (*7, 8*). The interplay between histone acetyltransferases (HATs) and HDACs acts as a dynamic regulatory mechanism, with these enzymes functioning as writer and eraser proteins that modulate the acetylation status at distinct histone sites (*9*). Reader proteins, including bromodomain-containing proteins, specifically recognize acetylated sites and recruit transcriptional complexes to target genes, thereby determining their activation state. Notably, various histone H3 variants, characterized by subtle alterations in their tail domains, have been shown to play unique roles in regulating gene expression and plant development. For instance, histone H3.3 is predominantly associated with transcriptionally active regions during Arabidopsis development, whereas the H3.1 variant is more commonly found in inactive heterochromatic regions (*10*).

In Arabidopsis, the HDAC family comprises three classes: HDA1/RPD3-type, sirtuin, and HD-tuin subfamilies, consisting of 18 genes. Each HDAC has diversified its function and plays pivotal roles in various biological processes (*11*). As a member of the RPD3-type subfamily of class I histone deacetylases, HDA19, together with HDA6 and HDA9, is involved in the epigenetic regulation of gene expression. HDA19 deficiency leads to a high tolerance towards salt, dehydration, and heat stresses with slower development and reduced fertility (*11-13*). Despite growing recognition of the importance of HDA19 and its homologue in rice in stress responses (*14*), its substrates remain unclear. Most studies have focused on its role in regulating specific histone marks, such as H3K9ac, H3K9K14ac, and H3K9K18ac, which are commonly conserved among eukaryotes including yeast, plants, and mammals (*15*).

Recent mass spectrometry-based (MS) lysine acetylome studies in plants and mammalian cell culture using the RPD3-class inhibitor apicidin have comprehensively revealed significant changes in the nuclear acetylome when the activity of this class of deacetylases is modulated, affecting both histone and non-histone proteins (*16, 17*). The diversification of primary structures of plant histones (H2A; 6 variants and 13 genes, H2B; 11 variants and 11 genes, H3; 9 variants and 15 genes in Arabidopsis), except for H4 (*18*), and the emergence of plant specific accessory proteins like angiosperm-specific HDA19-interacting homologous proteins (HDPIs) (*19*), highlight the need for a comprehensive dissection of *hda19* mutants to uncover acetylation marks through which HDA19 dominantly regulates stress responses. In this work, we found that di-acetylation of H3.3 at K27/K36 mediates salt tolerance, whereas the absence of HDA19 has only a minor effect on canonical acetylation marks, including H3K9ac, H3K9K14ac, and H3K9K18ac. Furthermore, lysine-to-glutamine (K/Q) substitutions, which mimic the acetylated states at this novel di-

acetylation site, induce the expression of late embryogenesis abundant (LEA) proteins, thereby conferring salt stress tolerance comparable to that observed in *hda19* mutants.

Results

Rfhda19, a novel *hda19* allele with reverted fertility and maintained stress tolerance

Our previous work showed that the *hda19-3* mutant, which is deficient in HDA19, exhibits a severe defective phenotype in reproductive organ-formation and fertility, as well as a salt and drought stress tolerance phenotype. In this study, we aim to identify the *in vivo* HDA19 substrates by mass spectrometry-based acetylome profiling to elucidate the mechanism by which *hda19* mutants acquire their tolerance. The slow growth of the *hda19-3* mutant made it challenging to directly compare them with Col-0 wild-type (WT) plants. To address this issue, we screened for additional *hda19* mutant alleles that retained their stress tolerance but had a less severe growth defect. Among the progeny of a previously described genome-edited *hda19-7* line (*13*), which contains a G insertion at 79 nucleotides of the *HDA19* coding sequence, we identified a revertant in fertility, designated *Rfhda19* for this reason. This *Rfhda19* mutant contains an insertion of plasmid-like foreign DNA into the genomic region around the translational initiation site of HDA19, resulting in the deletion of 57 nucleotides from the HDA19 coding sequence, which leads to a modified N-terminus of the protein (fig. S1A). *Rfhda19* retains similar stress resistance to *hda19-3* and exhibits partial recovery to semi-fertility from almost sterile phenotypes, enabling better growth and allowing for a more suitable comparison to WT plants (Fig. 1A, fig. S1, B to D). To confirm that the phenotype is caused by the lack of active HDA19, the genomic DNA encompassing the coding sequence and proximal regulatory elements of *HDA19* was introduced into *Rfhda19*, and the resultant T_3 plants displayed decreased tolerance to salinity stress as WT plants (fig. S1E and F). To determine if the *Rfhda19* line also lacks an active HDA19 enzyme, we performed a pull-down analysis using the HDAC-trap mini-AsuHd, which enriches catalytically active HDACs by hydroxamic acid grafted onto a lysine-like scaffold (*20*). While HDA19 was highly enriched on mini-AsuHd from WT extracts, it was absent in *Rfhda19* mutants (fig. S2 and Data S1) due to its impaired activity.

Histone H3.3 and seed-specific proteins are hyperacetylated *in hda19*

To identify the *in vivo* protein substrates of HDA19, we analyzed the proteomes and acetylomes of five-day-old Arabidopsis seedlings from the two different lines lacking HDA19 (*hda19-3* and *Rfhda19)* compared to WT plants using a quantitative liquid chromatography mass spectrometry-based (LC-MS) proteomic approach. In total, 4989 and 4428 protein groups were quantified in at least two biological replicates in the *Rfhda19* and *hda19-3* versus WT comparisons, respectively. Moreover, 3726 and 3318 lysine acetylation (acK) sites were quantified on 1669 and 1465 unique protein groups, respectively (fig. S3 and fig. S4, Data S2 and S3). The majority of protein groups and 1912 lysine acetylation (acK) sites were common to both *hda19* deficient lines in these datasets (fig. S5). To reveal whether similar changes in protein and acK site abundance changes occur in both *hda19* mutant lines, we directly compared the regulation patterns between the two lines. Scatter plots illustrate a high degree of similarity between the two *hda19* mutants relative to WT, with 44 protein groups and 63 acK sites on 36 protein groups exhibiting strong increases in abundance in both lines ($\log_2$ FC > 1) (Fig. 1, B and C). Given this high degree of correlation of the proteome response in both lines, we combined them into a single group (*hda19*) and considered protein groups and acK sites quantified in six out of eight replicates for further statistical analysis. This combined analysis revealed 94 acK sites on 49 protein groups with significantly and more than two-fold increased hyperacetylation ($\log_2$ FC > 1, FDR < 5%) (Fig. 2, A and B, DataS4). The strongest increase in lysine acetylation (>16-fold) was observed for the seed storage protein CRUCIFERIN 4 (CRU4) and LEA29 (fig. S6). Only 11 of the 49 hyperacetylated proteins (AHL14, Ankyrin repeat family protein (AT2G26210), DNA-binding storekeeper protein-

related transcriptional regulator (AT4G00390), H3.3, LEA7, LEA25, LEA29, MAC7, PARP3, PWO1, SCS2B) are known to localize to the nucleus, and one (RAB18) to the nucleus and plasma membrane, according to SUBA5 (Fig. 2C). A sequence logo generated from the 94 hyperacetylated sites revealed a putative substrate motif for HDA19, characterized by lysine residues at positions -13, -2, and +11, and alanine residues at positions -3 and +1, and aspartic acid at position -1 surrounding the actual acetylation site (Fig. 2D). Functional enrichment analysis of the hyperacetylated proteins showed that the GO Component term "protein storage vacuole", the GO Function term "nutrient reservoir activity", and the UniProt Keyword "seed storage protein" were the three terms most enriched terms (Fig. 2E). Comparison of proteome and acK site abundance changes revealed a high correlation, with 24 protein groups exhibiting similar increases in acetylation and protein abundance in *hda19* compared to WT (Fig. 2F). However, 24 acK sites on 19 proteins showed an at least 2-fold stronger increase in lysine acetylation than in protein abundance. Among these 19 proteins, the histone protein H3.3 with two acetylation sites (K27 and K36) and multiple LEA proteins with various acK sites (LEA25 K300; LEA29 K38, K82, K111; LEA48 K153; RAB18/LEA51 K180) were identified.

Histone H3K27/36 acetylation is indispensable for salinity tolerance

Gene expression is heavily influenced by histone modifications, with even minor variations in histone sequences giving rise to distinct regulatory functions. In Arabidopsis, 50 genes encode 37 different histone proteins (*21*). We quantified 32 of those histone proteins at either the protein or acetylation level (DataS4). Due to the high lysine content of histone tails, tryptic peptides often carry more than one acK site. This is particularly important, as H3.3 hyperacetylation was only observed on peptides carrying di-acetylation at both K27 and K36, while peptides showing mono-acetylation only at K36 were slightly downregulated (Fig. 3A). Since the differences in amino acid sequences between the histone variants are relatively small, distinguishing between them is not always possible, especially for acK sites where the corresponding amino acid changes may not reside on the same tryptic peptide. In the case of H3.3, a single amino acid exchange from alanine to threonine between H3.1 and H3.3 can be found at position 31 (*21*), which is distinguishable in the MS/MS spectra of the di-acetylated peptide (Fig. 3B). H3.3 is often enriched at euchromatin regions and associated with active gene expression, whereas H3.1 is enriched in heterochromatin and associated with gene silencing (*22*). Both acetylome and immunoblotting analyses detected a significant increase in di-acetylation levels of lysines (K) 27 and 36 of histone H3.3 (H3.3K27/K36ac) in *hda19* compared to WT plants, although this increase was less pronounced in *Rfhda19* (Fig. 2F, Fig. 3, A and C). The difference between *hda19-3* and *Rfhda19* may be attributed to the fact that a truncated, non-active HDA19 protein might be generated in *Rfhda19*, although this was not detectable by LC-MS/MS analysis. Additionally, the difference could be caused by the slightly enhanced developmental speed of *Rfhda19* compared to *hda19*-3, particularly given that H3.3 enrichment patterns change during early development (*23*). Plants treated with trichostatin A (TSA), a pan-HDAC inhibitor, showed a 2-fold increase of acetylation at H3.3K27/K36ac compared to control conditions in the immunoblot analysis (Fig. 3C). Similarly, a previous MS-based analysis of apicidin treated plants showed a nearly 6-fold increase in di-acetylation of H3.3K27/K36ac (*16*). Higher acetylation levels of K27/K36 after inhibitor treatments may be explained by additional inhibition of HDA6, which is thought to work redundantly with HDA19 (*24*). In contrast to *Rfhda19* treated with salt, WT plants showed slightly decreased di-acetylation of K27 and K26 under the same conditions (Fig. 3A). This is consistent with a previously observed up-regulation of HDA19 activity upon salt stress in WT plants (*25*). Here we detected increased lysine acetylation on H3.3 only in the absence of HDA19 (Fig. 3A), indicating that HDA19 can distinguish between histone variants to regulate gene expression.

To confirm the role of H3.3K27/K36ac in response to salinity stress, we introduced two K to Q mutations at the 27 and 36 sites of histone HTR5, a variant of H3.3 in Arabidopsis. The replacement of lysine residues with glutamine (K→Q) is considered to mimic the acetylation mark due to the permanent abolishment of the positive charge (*26*). Three different genes, HTR4/5/8, encode H3.3 in Arabidopsis (*21*). Expression of HTR5:FLAG complemented the *htr4/5/8* mutant derived from *htr4/5*(-/-) *htr8*(+/-) progeny (fig. S7), indicating that FLAG-tagged HTR5 is functional, whereas constitutive expression of K27/K36Q in all three H3.3 variants appears lethal in Arabidopsis, as HTR5K27/K36Q:FLAG was detected only in an *htr4/5* background but not in *htr4/5/8* progeny. Plants expressing HTR5K27/K36Q:FLAG under the control of the gene-specific promoter and terminator showed salinity stress tolerance (Fig. 3, D and E). These data indicate that H3.3K27/K36ac regulates the response to salinity stress in Arabidopsis.

Identification of HDA19 interaction partners in Arabidopsis seedlings

Previous studies have identified several proteins that interact with HDA19 in chromatin-modifying complexes. To further investigate the interactions of HDA19, we performed a quantitative pull-down analysis of MycHDA19 expressed in *hda19-6* seedlings compared to WT plants via LC-MS. In total, 203 protein groups were quantified in at least two out of four replicates, and 22 of those protein groups were significantly enriched ($\log_2$ fold-change > 1 and adjusted p-values (FDR) < 0.05) in MycHDA19 compared to WT, including HDA19 itself (Fig. 4, Data S5). Among these 22 proteins, nine localize to the nucleus and five to the cytosol, suggesting that HDA19 might also function in more than one compartment. We detected multiple members of the known HDA19-SIN3 complex, including HISTONE DEACETYLASE COMPLEX 1 (HDC1), MSI1, SIN3-like (SNL) proteins 1-6 (*27-30*). Recently, three new angiosperm specific members of the HDA19-SIN3 complex called HDIPs were identified (*19*). HDIP3 co-purified with MycHDA19 in this study, along with several previously unreported proteins (Fig. 4), including the small GTP-binding protein RAN1, which regulates nuclear-cytoplasmic transport (*31*), four ribosomal proteins, and the dynamin-related protein 2 family protein important for gametophyte development and biotic stress resistance (*32, 33*). These HDA19 interacting proteins are likely to play a crucial role in regulating stress responses through the modification of H3.3K27/K36ac.

Requirement of LEA proteins in enhancing salinity stress tolerance in *hda19* mutants

LEA proteins play crucial roles in protecting plants against environmental stresses, such as desiccation, drought and salinity. Despite their importance, the regulation of LEA proteins is not yet fully understood. In total, 22 out of 51 LEA proteins were quantified at either the protein or acK level (Fig. 5A). These proteins belong to different subfamilies, including LEA_1, LEA_2, LEA_3, LEA_4, dehydrins, and PvLEA18. LEA_4 family is the largest of these, comprising 19 LEA proteins, of which nine were found in this dataset (*34*). Here we report that the protein abundance of 11 LEA proteins and 33 acK sites of seven of these proteins were strongly upregulated in *hda19* mutants (DataS4). The strongest induction was primarily observed for the LEA_4 family members, with many proteins showing significant increases in both protein and acK site abundance. The highest increase was observed for LEA29 acK sites K38, K82, and K111, which showed an over 11-fold increase in the *hda19* mutants compared to WT plants (Data S4). LEA7, a paralog of LEA29 with preserved nucleotide similarity, was duplicated as a result of a whole-genome duplication event (*34*) and also exhibited increased protein abundance and acK levels in *hda19* mutants. In addition to the LEA_4 family proteins, the acetylation of the dehydrin RAB18/LEA51 was also strongly increased at K180 (Fig. 5A). Both LEA7 and LEA29 have been reported to be induced under salt and osmotic stress, and during treatment with the plant hormone abscisic acid (ABA) (*35*). RAB18 is also induced in response to salinity, ABA, and other environmental stresses (*34, 36*). To test whether these LEA proteins contribute to the enhanced salinity tolerance of *hda19* mutants, we generated higher-order mutants. The quadruple *lea7-1/lea29-1/rab18-1/Rfhda19*

mutants showed markedly reduced tolerance to 125 mM NaCl, with a survival rate of 36.7% (Fig. 5B), compared with 73.3% in *Rfhda19* mutants (Fig. 5B). To determine whether the mRNA expression of LEA7, LEA29, and RAB18 is regulated by H3.3K27/K36ac, we analyzed mRNA levels in plants expressing HTR5 K27/K36Q:FLAG. Their transcript abundance was significantly elevated in these plants relative to both WT and *htr4/5* mutant backgrounds (Fig. 5C). Together, these results indicate that LEA7, LEA29, and RAB18 proteins promote salinity tolerance in *hda19* mutants via H3.3K27/K36ac mediated gene expression regulation (Fig. 6).

Discussion

Our study revealed that the di-acetylation site H3.3K27/K36ac is a critical epigenetic mark regulated by HDA19, which plays a key role in salinity stress tolerance in Arabidopsis. Hyperacetylation of these amino acids was found to drive the up-regulation of LEA proteins at both the transcript and protein levels in *hda19* mutants, thereby conferring salt stress tolerance.

Histone modifications represent a "histone code" that recruits transcriptional regulators to activate or repress mRNA synthesis. These histone codes are regulated by writers (catalyzing modifications), erasers (removing modifications), and reader (recognizing modifications) proteins (*37, 38*). Elucidating the interactors of each histone code is essential for understanding their role in the respective biological processes. The acetyltransferase GCN5 may play an antagonistic role to HDA19 at H3.3K27/K36ac sites, as it has been shown to acetylate H3K27 and K36 in Arabidopsis to activate transcription in euchromatin (*39-41*). The opposing photomorphogenesis phenotypes observed in *gcn5* and *hda19* mutants were absent in a double mutant (*41*). Furthermore, HDA19 may influence the activity of the SAGA complex, as evidenced by the hyperacetylation of its subunits TAF5 and SCS2B in *hda19* mutants. In addition to HDA19, the Arabidopsis genome encodes for three other class I HDACs (HDA6, HDA7, and HDA9) (*11*), although HDA7 is considered to be a pseudogene due to the of loss of the Zn^{2+} binding site in the catalytic pocket (*42*). HDA9, another class I HDAC, is also thought to mediate H3K27 deacetylation (*43*). The mono-deacetylation of H3K27ac seems to be redundantly regulated by multiple enzymes. Our acetylome analysis furthermore revealed increased acetylation of the PWWP-DOMAIN INTERACTOR OF POLYCOMBS1 (PWO1) protein at residue K696. PWO1 regulates flowering, development, and nuclear size, and has been described as a putative histone reader protein that recruits multiple histone methyltransferases and maintains H3 methylation occupancy (*44, 45*). Given that PWO1 has also been identified as a potential HDA19 interacting partner in an HDA19-GFP pull-down (*46*), it is possible that HDA19 regulates the activity of PWO1 via deacetylation. Further characterization of novel HDA19 substrates and interacting proteins will enhance our understanding of how plants regulate stress responses through H3.3K27/K36ac and why HDA19 dominantly mediates di-acetylation of H3.3K27/K36ac.

In addition to H3.3K27/36, we identified further 48 putative substrate proteins with a consensus acetylation motif for HDA19, including 38 proteins that are not known to localize to the nucleus (Figs. 1 and 2). This raises questions about the subcellular localization of HDA19 and its substrates that require further investigation. Previously, HDA19 was reported to be exclusively localized to the nucleus (*47*); however maize RPD3-type HDACs have also been reported to have both a nuclear and cytoplasmic localization (*48*), and a significant proportion of Arabidopsis HDA9 was also found in the cytoplasm (*49*). Furthermore, human class I HDAC3 has been shown to reside in both the nucleus and cytosol, owing to its possession of a nuclear export signal (*50*). Additionally, human HDAC1-3 have been detected in the endoplasmic reticulum, where they play a role in modulating the unfolded protein response (*51*).

Our data show that the hyperacetylation of histone H3.3 K27/K36 leads to an up-regulation of LEA mRNA abundance (Fig. 5, B and C). Furthermore, we demonstrate that three LEA proteins, which are ABA-responsive genes (*34*), are essential for the salt tolerance conferred by HDA19

deficiency. Initially, LEA proteins were described to accumulate during seed maturation, where they help protect cells during seed desiccation (*52, 53*). Expression of LEA proteins has been detected in non-plant taxa, various plant organs, and under different stress conditions, suggesting a broader role for LEA proteins in stress responses (*34, 54, 55*). The strong hyperacetylation of LEA proteins, particularly LEA29, implies a more direct role for HDA19 in regulation LEA proteins. Although no enzymatic functions have been reported for LEA proteins to date, multiple models have been proposed to explain their involvement in stress tolerance. These models include binding and potentially stabilizing membranes or binding directly to proteins to prevent aggregation in a chaperone-like manner (*56, 57*). Additionally, a molecular shield function has been suggested, where LEA proteins contribute to molecular crowding, preventing molecule collisions (*58*). LEA proteins, such as LEA7 and LEA29, are highly disordered in solution but form a high number of α-helices during drying (*59, 60*). LEA29 has been shown to form homodimers and heterodimers with LEA7 in tobacco leaves (*61*). The secondary structure formation of LEA7 appears to be partly dependent on the presence of membranes, although a stabilizing effect on liposomes during drying was not observed (*60, 62*). A protective effect of LEA7 on the activity of lactate dehydrogenase during freezing and drying was observed (*62*). Therefore, the accumulation and acetylation of LEA29, LEA7, and RAB18 may contribute to the protection of membranes and proteins under stress conditions. Elucidating the mode of action of these acetylated LEA proteins in the future will provide valuable insights into tolerance of salinity stress in plants.

Overall, our findings suggest that ABA signaling is the key pathway controlled by HDA19 via the regulation of histone H3.3 K27/K36 di-acetylation in response to salinity stress. Recently, angiosperm-specific HDA19-interacting proteins (HDPIs) have been identified (*19*) and were also found in our HDA19 seedling interactome (Fig. 4), along with other new interacting proteins. Although HDACs are highly conserved among eukaryotes, the study of plant-specific HDA19-interacting proteins, such as HDPIs, will provide further insights into the molecular mechanisms of ABA signaling regulation through H3.3 K27/K36ac.

In summary, our study identifies the histone H3.3 di-acetylation site K27/K36 as a key mediator of salinity stress tolerance, regulated by HDA19. Further characterization and identification of the coordinators of H3.3 K27/K36ac will reveal specific targets for manipulating stress responses, as HDACs represent a promising target for chemical intervention in various biological processes.

Materials and Methods

Plant material and growth conditions

Arabidopsis thaliana (L.) Heynh. (Columbia: Col-0 as wild-type accession in this study), *hda19-3* (*63*); SALK_139445, *htr4htr5-1* (*64*); SALK_042781, *htr8-3* (*64*); SALK_087850, *lea7-1* (*65*); SALK_205942 (Col-0), *hda19-7* [in 79G, a genome-edited allele in Col-0 by previous study (*13*)], Reverted fertility in *hda19-7* (*Rfhda19*) (fig. S1A), *lea29-1* (in 104T, a genome-edited allele) (fig. S8A) and *rab18-1* (in 223A, a genome-edited allele) (fig. S8B) and were used in the course of this study. Plants treated with trichostatin A (T1952, Sigma–Aldrich, St. Louis, MO) were prepared as described previously (*13*). After surface-sterilization with sodium hypochlorite, followed by two rinses with distilled water, seeds were floated on 1 mL liquid media (half-strength MS medium with 0.5% MES and 0.1% agar, pH 5.7) at 4 °C for 48 h in 24-well tissue culture plates (TPP; Trasadingen, Switzerland). After germination, the plants in the 24-well tissue culture plates were placed in a growth chamber at 22 °C with a long-day photoperiod (16h/8h light/dark cycle) at 50–100 $\mu E\ m^{-2}\ s^{-1}$. For the acetylome and pull-down analyses, 5-d-old-plants were harvested, and for the proteome analysis of the early salt stress response, plants were exposed to salinity stress for 2 h before harvesting. After harvesting of four biological replicates each, plants were immediately flash frozen in liquid nitrogen and stored at -80 °C. The plant samples for proteomic analysis were dried

using a freeze dryer (FRD-830D, IWAKI CO., LTD., Tokyo, Japan) for 24 hours. Developmental stages of stamen and pistil in *Rfhda19* and wild-type plants were referred to Smyth et al 1990 (*66*).

Generation of mutant lines using the CRISPR/Cas9 system

The *rab18-1* and *lea29-1* alleles were generated by genome editing as described previously (figure S8) (*67, 68*). The sgRNAs used for mutagenesis were designed using the CRISPRdirect program (*69*). To express a single guide RNA (sgRNA) and CRISPR/Cas9 protein, pZH_OsU3gYSA_FFCas9 and pUC_AtU6oligo vectors were used for targeted mutagenesis in RAB18 and LEA29. The sgRNA information used to target them is presented in table S2.

Generation of complement lines expressing H3.3 K/Q mutant.

K to Q substitutions in K27 and K36 of HTR5 coding sequence were introduced by PCR-based site-directed mutagenesis (*70*), and fused in reading frame with a C-terminal FLAG (DYKDHDGDYKDHIDYKDDDDK). Genomic DNA of HTR5 was used and the construct was first cloned into a pENTR/DTOPO vector (Thermo Fisher Scientific, Plaquemine, LA). The resultant DNA was used as a template for mutagenesis. The HTR5K27/K36Q:FLAG coding gene was expressed under the control of its own promoter and terminator in the *htr4htr5-1* mutant background as follows. Amplified PCR products of promoter, gene body, and terminator fragments were assembled into plant expression vector pHGW (*71*), by HiFi DNA Assembly (New England Biolabs, Ipswich, MA). Primer pairs used for mutagenesis and cloning are shown in table S3. Agrobacterium tumefaciens strain C58C1 was transformed by the pHGW binary vector and used for floral dip transformation in *htr4/5* according to the method of Clough and Bent (*72*).

Evaluation of salinity tolerance

When plants were 5 days old (counted from seed germination), 20 µL or 25 µL of 5 M NaCl were added to each well, yielding final concentrations of 100 mM or 125 mM NaCl per well, respectively, while control plants received no salt. Percent survival was assessed five days later using three biological replicates, each containing 15 plants. Plants with green true leaves were scored as survivors. Survival rates were statistically analyzed by a one-way ANOVA in the GraphPad Prism version 10. 2. 3 for Windows (GraphPad Software, San Diego, CA).

Reverse transcription quantitative polymerase chain reaction (RT-qPCR) analysis

First-strand cDNA was synthesized from 250 ng total RNA extracted from 10 plants per condition using random primers and ReverTra Ace (TOYOBO, Osaka, Japan). Transcript levels were analyzed using Fast SYBR Green Master Mix (Applied Biosystems, Foster City, CA) and the StepOnePlus Real-Time PCR System (Applied Biosystems, Foster City, CA) according to the manufacturer's protocols and previous study (*73*). Gene-specific primers were designed using the PrimerQuest tool (http://sg.idtdna.com/primerquest/Home/Index). The relevant primers are listed in table S4. Changes in gene expression (n=6) were statistically analyzed by a one-way ANOVA in the GraphPad Prism version 10. 2. 3 for Windows (GraphPad Software, San Diego, CA).

Immunoblotting

Tissue powder from ten five-day-old plants was solubilized in 2 x Laemmli buffer (100 µl/ 10 plants) under reducing conditions (200 mM DTT or 2% β-mercaptoethanol) and heated at 95 °C for 3 min. Protein extracts were separated by sodium dodecyl sulfate polyacrylamide gel electrophoresis on 15% bis-Tris gels (Nacalai Tesque, Kyoto, Japan) and subsequently transferred to TransBlot Turbo mini-size PVDF membranes (Bio-Rad, Hercules, CA). The membranes were blocked for 1 h with 5% skim milk, incubated overnight at 4 °C with the primary antibody, and then incubated for 1 h with the anti-rabbit secondary antibody (NA934, Cytiva, Marlborough, MA, USA) or anti-mouse (NA931, Cytiva) IgG secondary antibody conjugated to horseradish peroxidase. Immunoreactive proteins were detected using Chemi-Lumi One Super (Nacalai Tesque, Japan), and images were acquired with an ImageQuant800 scanner (Cytiva). Band intensities were

quantified with ImageJ software. Equal protein loading was verified by probing for histone H3. Primary antibody dilutions were as follows: H3.3 (HTR4/HTR5/HTR8) K27/K36ac, 1: 500 (polyclonal antibody raised against H3.3K27acK36ac in this study); H3, 1:2,000 (polyclonal, Abcam, Cambridge, MA, 1791); and Myc-tag, 1:1,000 (monoclonal, MBL, Japan M185-3L). Synthetic peptides [CKAARKAcSAPTTGGVKAcKP] were used as antigen to produce polyclonal antibodies against H3.3K27/K36ac (Scrum, Tokyo, Japan).

Enrichment of active HDACs using AsuHd probes

Plant material was homogenized and suspended in extraction buffer (EB) containing 50 mM HEPES (pH 7.5), 150 mM NaCl, 10% [v/v] glycerol, 5 mM ascorbate, 0.25% [v/v] Triton X-100, and cOmplete™ EDTA-free Protease Inhibitor Cocktail (Roche). Extracts were incubated at 4 °C for 1 h with constant agitation, and cell debris was pelleted by centrifugation at 18,000 x *g* for 25 min at 4 °C. Protein concentrations in the supernatants were determined using the Pierce 660 nm Protein Assay (Thermo Fisher Scientific). Resins with mini-AsuHd (HDAC trap) and mini-Lys peptide (control) probes (*20*), were equilibrated 3x with 600 µL wash buffer (WB) (50 mM Hepes pH 7.5, 150 mM NaCl, 10% [v/v] glycerol, 5 mM ascorbate). Equal amounts of each sample were incubated overnight at 4 °C with both mini-AsuHD and mini-Lys beads under constant agitation. Beads were transferred onto a micro-centrifugal filter system (amchro GmbH) and washed 5x with 250 µL WB. An on-bead trypsin digestion was performed as described previously (*25*). Peptides were desalted using C18 Stage tips (*74*) prior LC-MS/MS analysis.

Myc pulldown

Plant material was homogenized and suspended in EB buffer as described above. EZview™ Red Anti-c-Myc Affinity Gel (Merck Millipore, Darmstadt, Germany) was equilibrated 3x with WB (50 mM Tris pH 7.5, 150 mM NaCl, 10% [v/v] glycerol, 2 mM EDTA). Protein extracts were incubated on beads over-night at 4 °C with constant agitation. Beads were collected by slow centrifugation (500 x *g*) at 4 °C and washed 3x with 1 mL WB for 5 min with constant agitation. Proteins were eluted two times with 30 µL 0.1% (v/v) TFA for 5 min and collected by gentle centrifugation. An in-solution trypsin digestion was performed as described previously. For total proteome analysis, peptides from input samples were prepared using small-scale filter-aided sample preparation (FASP) as described previously (*75*).

Quantitative proteomics and lysine acetylome

Proteins were extracted from plant material under denaturing conditions as described previously (*76*). DTT was replaced with tris(2-carboxyethyl)phosphine (TCEP). Proteins were processed using single-pot, solid-phase-enhanced sample preparation (SP3) (*77*). After the tryptic digest, peptides were labeled using tandem mass tags (TMT) (*78*). TMT10plex™ (Thermo Fisher Scientific) reagents were used. Samples were randomized within each TMT set. Each channel was assigned to one genotype or treatment, or a pool of all samples for normalization purposes. Peptides were resuspended in TBS buffer (50 mM Tris–HCl, 150 mM NaCl, pH 7.6). A more than 98% labeling efficiency was confirmed by LC-MS/MS analysis and samples were pooled afterwards. 30 µg of pooled peptides was stored for whole proteome analysis. Lysine-acetylated peptides were enriched using PTMScan® Acetyl-Lysine Motif [Ac-K] Immunoaffinity Beads (Cell Signaling Technology) as described previously (*35*). All total proteome and acetylome samples were desalted using SDB-RPS Stage tips (*76*), eluted in three separate fractions, and dried using a vacuum concentrator.

LC-MS/MS data acquisition

Peptides were resuspended in 2% (v/v) acetonitrile and 0.1% (v/v) TFA. Aceylome, proteome and HDAC pulldown samples were measured using an EASY-nLC 1200 system coupled to an Exploris 480 mass spectrometer (Thermo Fisher Scientific). Myc pulldown and corresponding

input samples were measured using an EASY-nLC 1200 system coupled to an Q Exactive HF mass spectrometer (Thermo Fisher Scientific). The peptides were separated on 20 cm fritless silica emitters with a 0.75 µm inner diameter (CoAnn). Emitters were packed in-house with reversed-phase 1.9 µm ReproSil-Pur C_{18}-AQ (Dr Maisch GmbH). A 115 min (78 min for Myc pulldown) LC gradient using 0.1% (v/v) formic acid as buffer A and 80% (v/v) acetonitrile, 0.1% (v/v) formic acid as buffer B was used. Data acquisition settings for all experiments are listed in table S5.

Data analysis

LC-MS/MS raw data were analyzed with the MaxQuant (MQ) software (v 2.4.14.0, https://maxquant.net) (*79*). The raw data was searched against an in house curated Araport11 database including organellar specific proteins after processing based on targetP2 (*80*), and a database containing mitochondria-encoded proteins after RNA editing (*81, 82*). Common contaminants lists and a reverse decoy database were enabled in the MaxQuant software settings. Proteome and acetylome samples of *hda19-3* and *Rfhda19* were analyzed in the same MQ search using dedicated parameter groups. All pull-down samples and respective inputs were analyzed in. the same MQ search using dedicated parameter groups. Carbamidomethylation of cysteines was set as fixed modification and oxidation of methionine and acetylation of protein N-termini were set as variable modifications. Trypsin was selected as protease. For acetylome samples, lysine acetylation was set as variable modifications, the number of max. missed cleavages was set to 3 (2 for all other samples), and PTM was set as TRUE. Match between runs was activated for all samples. min. score for modified peptides was set to 35 for the acetylome search as reported previously (*16*). MS^2-based quantification was activated and set to TMT10plex for acetylome and corresponding proteome samples. TMT correction factors were adjusted to the specific TMT batch, filter by PIF was activated, and normalization was set to “Weighted ratio to reference channel”. Re-quantify was enabled, as well as separate variable modifications for first search. For pull-down and respective input samples label-free quantification (LFQ) was enabled and the LFQ min. ratio count was set as 1. Separate LFQ in parameter groups was activated. iBAQ was enabled. min. peptide length was set to 7 for all searches. Both PSM and protein FDR were set to 0.01.

MQ output tables were imported into Perseus (v 2.0.11.0, https://maxquant.net/perseus/) (*83*). Contaminants and reverse hits were removed by filtering. Proteins only identified by site were removed by filtering for pull-down samples only. LFQ intensities and corrected reporter intensities were $\log_2$ transformed. Protein groups and acK sites were filtered for minimum valid values as indicated in DataS1-5. TMT samples were normalized by median subtraction. Missing values were imputed following normal distribution in Myc input samples (width = 0.3, down shift = 1.8), Myc pull-down WT control (width = 0.5, down shift = 2.2), and HDAC pull-down mini-Lys controls (width = 0.4, down shift = 1.5). Data was exported from Perseus and imported into R (v 4.4.1). Statistical analysis was performed using the *limma* package (v 3.60.6) (*84*). The *p*-value was adjusted with Benjamini-Hochberg. Packages dplyr (v 1.1.4), tidyr (v 1.3.1), reshape2 (v 1.4.4), stringi (v 1.8.4), and stringr (v 1.5.1) were used for data processing. Results were visualized using the packages ggplot2 (v 3.5.2) and ggrepel (v 0.9.6). SUBAcon annotations of protein subcellular localizations were retrieved from the SUBA5 database (*85*). Sequence logo of significantly upregulated acK sites (*hda19* vs. WT, $\log_2$ FC > 1, FDR < 0.05) was analyzed using the iceLogo software (*86*). The unregulated acK sites with a $\log_2$ FC < 1 were used as a negative set. A *p*-value cut-off of 0.05 was used. Functional enrichment analysis was performed using the Proteins with Values/Ranks function of stringDB (*87*). A rank value was calculated by multiplying the $\log_2$ acK FC with the $-\log_{10}$(adjusted *p*-value). For proteins with multiple acK sites, the site with the highest rank was used. GO cellular component, GO biological process, KEGG, UniProt Keywords were considered. Only terms showing an increase in their abundance were used. String Network analysis was done using Cytoscape (v 3.10.2) together with the stringApp (v 2.2.0) and the Omics Visualizer (v 1.3.1) (*88-90*). The confidence cut-off was set to 0.7. Histone variants have been annotated based

on Probst et al., 2020 (*21*), and LEA proteins based on Hundertmark and Hincha, 2008 (*34*). The localization of LEA proteins was referred to Candat et al 2014 (*91*).

References

1. H. Le, C. H. Simmons, X. Zhong, Functions and mechanisms of histone modifications in plants. *Annu Rev Plant Biol* **76**, 551-578 (2025). doi:10.1146/annurev-arplant-083123-070919
2. M. Ueda, M. Seki, Histone modifications form epigenetic regulatory networks to regulate abiotic stress response. *Plant Physiol* **182**, 15-26 (2020). doi:10.1104/pp.19.00988
3. J. A. Long, C. Ohno, Z. R. Smith, E. M. Meyerowitz, TOPLESS regulates apical embryonic fate in *Arabidopsis*. *Science* **312**, 1520-1523 (2006). doi:10.1126/science.1123841
4. P. B. Talbert, S. Henikoff, Histone variants--ancient wrap artists of the epigenome. *Nat Rev Mol Cell Biol* **11**, 264-275 (2010). doi:10.1038/nrm2861
5. T. Kouzarides, Chromatin modifications and their function. *Cell* **128**, 693-705 (2007). doi:10.1016/j.cell.2007.02.005
6. B. D. Strahl, C. D. Allis, The language of covalent histone modifications. *Nature* **403**, 41-45 (2000). doi:10.1038/47412
7. V. G. Allfrey, R. Faulkner, A. E. Mirsky, Acetylation and methylation of histones and their possible role in the regulation of rna synthesis. *Proc Natl Acad Sci U S A* **51**, 786-794 (1964). doi:10.1073/pnas.51.5.786
8. T. J. R. Penke, D. J. McKay, B. D. Strahl, A. G. Matera, R. J. Duronio, Functional redundancy of variant and canonical histone H3 lysine 9 modification in *Drosophila*. *Genetics* **208**, 229-244 (2018). doi:10.1534/genetics.117.300480
9. M. D. Shahbazian, M. Grunstein, Functions of site-specific histone acetylation and deacetylation. *Annu Rev Biochem* **76**, 75-100 (2007). doi:10.1146/annurev.biochem.76.052705.162114
10. H. Wollmann *et al.*, Dynamic deposition of histone variant H3.3 accompanies developmental remodeling of the *Arabidopsis* transcriptome. *PLoS Genet* **8**, e1002658 (2012). doi:10.1371/journal.pgen.1002658
11. C. Hollender, Z. Liu, Histone deacetylase genes in *Arabidopsis* development. *J Integr Plant Biol* **50**, 875-885 (2008). doi:10.1111/j.1744-7909.2008.00704.x
12. M. Ueda *et al.*, Versatility of HDA19-deficiency in increasing the tolerance of Arabidopsis to different environmental stresses. *Plant Signal Behav* **13**, e1475808 (2018). doi:10.1080/15592324.2018.1475808
13. M. Ueda *et al.*, The distinct roles of class I and II RPD3-like histone deacetylases in salinity stress response. *Plant Physiol* **175**, 1760-1773 (2017). doi:10.1104/pp.17.01332
14. Y. Wu *et al.*, OsHDAC1 deacetylates the aldehyde dehydrogenase OsALDH2B1, repressing *OsGR3* and decreasing salt tolerance in rice. *Plant Physiol* **198**, (2025). doi:10.1093/plphys/kiaf149
15. M. Luo, K. Cheng, Y. Xu, S. Yang, K. Wu, Plant responses to abiotic stress regulated by histone deacetylases. *Front Plant Sci* **8**, 2147 (2017). doi:10.3389/fpls.2017.02147
16. M. Hartl *et al.*, Lysine acetylome profiling uncovers novel histone deacetylase substrate proteins in *Arabidopsis*. *Mol Syst Biol* **13**, 949 (2017). doi:10.15252/msb.20177819
17. C. Scholz *et al.*, Acetylation site specificities of lysine deacetylase inhibitors in human cells. *Nat Biotechnol* **33**, 415-423 (2015). doi:10.1038/nbt.3130
18. R. Nunez-Vazquez, B. Desvoyes, C. Gutierrez, Histone variants and modifications during abiotic stress response. *Front Plant Sci* **13**, 984702 (2022). doi:10.3389/fpls.2022.984702

19. N. Liu *et al.*, Essential angiosperm-specific subunits of HDA19 histone deacetylase complexes in Arabidopsis. *EMBO J* **44**, 3521-3546 (2025). doi:10.1038/s44318-025-00445-w
20. A. Dose *et al.*, Interrogating substrate selectivity and composition of endogenous histone deacetylase complexes with chemical probes. *Angew Chem Int Edit* **55**, 1192-1195 (2016). doi:10.1002/anie.201508174
21. A. V. Probst, B. Desvoyes, C. Gutierrez, Similar yet critically different: the distribution, dynamics and function of histone variants. *J Exp Bot* **71**, 5191-5204 (2020). doi:10.1093/jxb/eraa230
22. H. Stroud *et al.*, Genome-wide analysis of histone H3.1 and H3.3 variants in *Arabidopsis thaliana*. *Proc Natl Acad Sci U S A* **109**, 5370-5375 (2012). doi:10.1073/pnas.1203145109
23. T. Zhao *et al.*, Histone H3.3 deposition in seed is essential for the post-embryonic developmental competence in Arabidopsis. *Nat Commun* **13**, 7728 (2022). doi:10.1038/s41467-022-35509-6
24. M. Tanaka, A. Kikuchi, H. Kamada, The Arabidopsis histone deacetylases HDA6 and HDA19 contribute to the repression of embryonic properties after germination. *Plant Physiol* **146**, 149-161 (2008). doi:10.1104/pp.107.111674
25. P. Tilak *et al.*, Proteome-wide lysine acetylation profiling to investigate the involvement of histone deacetylase HDA5 in the salt stress response of Arabidopsis leaves. *Plant J* **115**, 275-292 (2023). doi:10.1111/tpj.16206
26. A. Hecht, T. Laroche, S. Strahl-Bolsinger, S. M. Gasser, M. Grunstein, Histone H3 and H4 N-termini interact with SIR3 and SIR4 proteins: a molecular model for the formation of heterochromatin in yeast. *Cell* **80**, 583-592 (1995). doi:10.1016/0092-8674(95)90512-x
27. C. Feng *et al.*, Arabidopsis RPD3-like histone deacetylases form multiple complexes involved in stress response. *J Genet Genomics* **48**, 369-383 (2021). doi:10.1016/j.jgg.2021.04.004
28. S. Mehdi *et al.*, The WD40 domain protein MSI1 functions in a histone deacetylase complex to fine-tune abscisic acid signaling. *Plant Cell* **28**, 42-54 (2016). doi:10.1105/tpc.15.00763
29. G. Perrella *et al.*, Histone deacetylase complex1 expression level titrates plant growth and abscisic acid sensitivity in *Arabidopsis*. *Plant Cell* **25**, 3491-3505 (2013). doi:10.1105/tpc.113.114835
30. Z. Wang *et al.*, *Arabidopsis* paired amphipathic helix proteins SNL1 and SNL2 redundantly regulate primary seed dormancy via abscisic acid-ethylene antagonism mediated by histone deacetylation. *Plant Cell* **25**, 149-166 (2013). doi:10.1105/tpc.112.108191
31. S. de Boor *et al.*, Small GTP-binding protein Ran is regulated by posttranslational lysine acetylation. *Proc Natl Acad Sci U S A* **112**, E3679-3688 (2015). doi:10.1073/pnas.1505995112
32. S. K. Backues, D. A. Korasick, A. Heese, S. Y. Bednarek, The *Arabidopsis* dynamin-related protein2 family is essential for gametophyte development. *Plant Cell* **22**, 3218-3231 (2010). doi:10.1105/tpc.110.077727
33. J. M. Smith *et al.*, Loss of *Arabidopsis thaliana* Dynamin-Related Protein 2B reveals separation of innate immune signaling pathways. *PLoS Pathog* **10**, e1004578 (2014). doi:10.1371/journal.ppat.1004578
34. M. Hundertmark, D. K. Hincha, LEA (late embryogenesis abundant) proteins and their encoding genes in *Arabidopsis thaliana*. *BMC Genomics* **9**, 118 (2008). doi:10.1186/1471-2164-9-118

35. P. S. Zhao *et al.*, Overexpression of *AtLEA3-3* confers resistance to cold stress in *Escherichia coli* and provides enhanced osmotic stress tolerance and ABA sensitivity in *Arabidopsis thaliana*. *Mol Biol+* **45**, 785-796 (2011). doi:10.1134/S0026893311050165
36. V. Lang, E. T. Palva, The expression of a *rab*-related gene, *rab18*, is induced by abscisic acid during the cold acclimation process of *Arabidopsis thaliana* (L.) Heynh. *Plant Mol Biol* **20**, 951-962 (1992). doi:10.1007/BF00027165
37. M. M. Zhou, P. A. Cole, Targeting lysine acetylation readers and writers. *Nat Rev Drug Discov* **24**, 112-133 (2025). doi:10.1038/s41573-024-01080-6
38. E. Seto, M. Yoshida, Erasers of histone acetylation: the histone deacetylase enzymes. *Cold Spring Harb Perspect Biol* **6**, a018713 (2014). doi:10.1101/cshperspect.a018713
39. C. Chen *et al.*, Cytosolic acetyl-CoA promotes histone acetylation predominantly at H3K27 in *Arabidopsis*. *Nat Plants* **3**, 814-824 (2017). doi:10.1038/s41477-017-0023-7
40. W. Mahrez *et al.*, H3K36ac Is an evolutionary conserved plant histone modification that marks active genes. *Plant Physiol* **170**, 1566-1577 (2016). doi:10.1104/pp.15.01744
41. M. Benhamed, C. Bertrand, C. Servet, D. X. Zhou, *Arabidopsis GCN5*, *HD1*, and *TAF1*/*HAF2* interact to regulate histone acetylation required for light-responsive gene expression. *Plant Cell* **18**, 2893-2903 (2006). doi:10.1105/tpc.106.043489
42. K. Saharan, S. Baral, N. H. Shaikh, D. Vasudevan, Structure-function analyses reveal *Arabidopsis thaliana* HDA7 to be an inactive histone deacetylase. *Curr Res Struct Biol* **7**, 100136 (2024). doi:10.1016/j.crstbi.2024.100136
43. X. Zeng *et al.*, HISTONE DEACETYLASE 9 functions with Polycomb silencing to repress *FLOWERING LOCUS C* Expression. *Plant Physiol* **182**, 555-565 (2020). doi:10.1104/pp.19.00793
44. M. L. Hohenstatt *et al.*, PWWP-DOMAIN INTERACTOR OF POLYCOMBS1 interacts with Polycomb-Group Proteins and histones and regulates Arabidopsis flowering and development. *Plant Cell* **30**, 117-133 (2018). doi:10.1105/tpc.17.00117
45. P. Mikulski *et al.*, The chromatin-associated protein PWO1 interacts with plant nuclear lamin-like components to regulate nuclear size. *Plant Cell* **31**, 1141-1154 (2019). doi:10.1105/tpc.18.00663
46. I. C. Velez-Bermudez, W. Schmidt, The interactome of histone deacetylase HDA19 in dark-grown Arabidopsis seedlings. *Front Plant Sci* **14**, 1296767 (2023). doi:10.3389/fpls.2023.1296767
47. P. M. Fong, L. Tian, Z. J. Chen, *Arabidopsis thaliana* histone deacetylase 1 (AtHD1) is localized in euchromatic regions and demonstrates histone deacetylase activity *in vitro*. *Cell Res* **16**, 479-488 (2006). doi:10.1038/sj.cr.7310059
48. S. Varotto *et al.*, Expression profile and cellular localization of maize Rpd3-type histone deacetylases during plant development. *Plant Physiol* **133**, 606-617 (2003). doi:10.1104/pp.103.025403
49. X. Chen *et al.*, POWERDRESS interacts with HISTONE DEACETYLASE 9 to promote aging in *Arabidopsis*. *Elife* **5**, (2016). doi:10.7554/eLife.17214
50. W. M. Yang, S. C. Tsai, Y. D. Wen, G. Fejer, E. Seto, Functional domains of histone deacetylase-3. *J Biol Chem* **277**, 9447-9454 (2002). doi:10.1074/jbc.M105993200
51. S. Kahali, B. Sarcar, A. Prabhu, E. Seto, P. Chinnaiyan, Class I histone deacetylases localize to the endoplasmic reticulum and modulate the unfolded protein response. *FASEB J* **26**, 2437-2445 (2012). doi:10.1096/fj.11-193706
52. L. Dure, 3rd, S. C. Greenway, G. A. Galau, Developmental biochemistry of cottonseed embryogenesis and germination: changing messenger ribonucleic acid populations as shown by in vitro and in vivo protein synthesis. *Biochemistry* **20**, 4162-4168 (1981). doi:10.1021/bi00517a033

53. G. A. Galau, D. W. Hughes, L. Dure, 3rd, Abscisic acid induction of cloned cotton late embryogenesis-abundant (*Lea*) mRNAs. *Plant Mol Biol* **7**, 155-170 (1986). doi:10.1007/BF00021327
54. J. Browne, A. Tunnacliffe, A. Burnell, Anhydrobiosis: plant desiccation gene found in a nematode. *Nature* **416**, 38 (2002). doi:10.1038/416038a
55. R. A. Stacy, R. B. Aalen, Identification of sequence homology between the internal hydrophilic repeated motifs of group 1 late-embryogenesis-abundant proteins in plants and hydrophilic repeats of the general stress protein GsiB of *Bacillus subtilis*. *Planta* **206**, 476-478 (1998). doi:10.1007/s004250050424
56. D. Kovacs, E. Kalmar, Z. Torok, P. Tompa, Chaperone activity of ERD10 and ERD14, two disordered stress-related plant proteins. *Plant Physiol* **147**, 381-390 (2008). doi:10.1104/pp.108.118208
57. M. C. Koag, R. D. Fenton, S. Wilkens, T. J. Close, The binding of maize DHN1 to lipid vesicles. Gain of structure and lipid specificity. *Plant Physiol* **131**, 309-316 (2003). doi:10.1104/pp.011171
58. S. Chakrabortee *et al.*, Intrinsically disordered proteins as molecular shields. *Mol Biosyst* **8**, 210-219 (2012). doi:10.1039/c1mb05263b
59. P. Knox-Brown *et al.*, Similar yet different-structural and functional diversity among *Arabidopsis thaliana* LEA_4 proteins. *Int J Mol Sci* **21**, (2020). doi:10.3390/ijms21082794
60. A. V. Popova, M. Hundertmark, R. Seckler, D. K. Hincha, Structural transitions in the intrinsically disordered plant dehydration stress protein LEA7 upon drying are modulated by the presence of membranes. *Biochim Biophys Acta* **1808**, 1879-1887 (2011). doi:10.1016/j.bbamem.2011.03.009
61. O. Ginsawaeng *et al.*, Subcellular localization of seed-expressed LEA_4 proteins reveals liquid-liquid phase separation for LEA9 and for LEA48 homo- and LEA42-LEA48 heterodimers. *Biomolecules* **11**, (2021). doi:10.3390/biom11121770
62. A. V. Popova, S. Rausch, M. Hundertmark, Y. Gibon, D. K. Hincha, The intrinsically disordered protein LEA7 from *Arabidopsis thaliana* protects the isolated enzyme lactate dehydrogenase and enzymes in a soluble leaf proteome during freezing and drying. *Biochim Biophys Acta* **1854**, 1517-1525 (2015). doi:10.1016/j.bbapap.2015.05.002
63. K. C. Kim, Z. Lai, B. Fan, Z. Chen, *Arabidopsis* WRKY38 and WRKY62 transcription factors interact with histone deacetylase 19 in basal defense. *Plant Cell* **20**, 2357-2371 (2008). doi:10.1105/tpc.107.055566
64. K. Liu *et al.*, Histone variant H3.3 controls *Arabidopsis* fertility by regulating male gamete development. *Plant Cell Physiol* **65**, 68-78 (2024). doi:10.1093/pcp/pcad119
65. W. D. Ong, Y. Makita, T. Miyazaki, M. Matsui, R. Shin, *Arabidopsis* transcriptomic analysis reveals cesium inhibition of root growth involves abscisic acid signaling. *Planta* **259**, 36 (2024). doi:10.1007/s00425-023-04304-y
66. D. R. Smyth, J. L. Bowman, E. M. Meyerowitz, Early flower development in *Arabidopsis*. *Plant Cell* **2**, 755-767 (1990). doi:10.1105/tpc.2.8.755
67. F. Fauser, S. Schiml, H. Puchta, Both CRISPR/Cas-based nucleases and nickases can be used efficiently for genome engineering in. *Plant J* **79**, 348-359 (2014). doi:10.1111/tpj.12554
68. S. Schiml, F. Fauser, H. Puchta, The CRISPR/Cas system can be used as nuclease for *in planta* gene targeting and as paired nickases for directed mutagenesis in Arabidopsis resulting in heritable progeny. *Plant J* **80**, 1139-1150 (2014). doi:10.1111/tpj.12704
69. Y. Naito, K. Hino, H. Bono, K. Ui-Tei, CRISPRdirect: software for designing CRISPR/Cas guide RNA with reduced off-target sites. *Bioinformatics* **31**, 1120-1123 (2015). doi:10.1093/bioinformatics/btu743

70. K. Ishizaki *et al.*, Development of gateway binary vector series with four different selection markers for the liverwort *Marchantia polymorpha*. *PLoS One* **10**, e0138876 (2015). doi:10.1371/journal.pone.0138876
71. M. Karimi, D. Inze, A. Depicker, GATEWAY vectors for *Agrobacterium*-mediated plant transformation. *Trends Plant Sci* **7**, 193-195 (2002). doi:10.1016/s1360-1385(02)02251-3
72. S. J. Clough, A. F. Bent, Floral dip: a simplified method for *Agrobacterium*-mediated transformation of *Arabidopsis thaliana*. *Plant J* **16**, 735-743 (1998). doi:10.1046/j.1365-313x.1998.00343.x
73. M. Ueda *et al.*, A pyrazole partially induces brassinosteroid-related gene expression, leading to salt stress sensitivity. *J Plant Growth Regul* **44**, 868-878 (2025). doi:10.1007/s00344-024-11496-4
74. J. Rappsilber, M. Mann, Y. Ishihama, Protocol for micro-purification, enrichment, pre-fractionation and storage of peptides for proteomics using StageTips. *Nat Protoc* **2**, 1896-1906 (2007). doi:10.1038/nprot.2007.261
75. J. R. Wisniewski, A. Zougman, N. Nagaraj, M. Mann, Universal sample preparation method for proteome analysis. *Nat Methods* **6**, 359-362 (2009). doi:10.1038/nmeth.1322
76. I. Lassowskat *et al.*, Dimethyl-labeling-based quantification of the lysine acetylome and proteome of plants. *Methods Mol Biol* **1653**, 65-81 (2017). doi:10.1007/978-1-4939-7225-8_5
77. C. S. Hughes *et al.*, Single-pot, solid-phase-enhanced sample preparation for proteomics experiments. *Nat Protoc* **14**, 68-85 (2019). doi:10.1038/s41596-018-0082-x
78. J. Zecha *et al.*, TMT labeling for the masses: A robust and cost-efficient, in-solution labeling approach. *Mol Cell Proteomics* **18**, 1468-1478 (2019). doi:10.1074/mcp.TIR119.001385
79. S. Tyanova, T. Temu, J. Cox, The MaxQuant computational platform for mass spectrometry-based shotgun proteomics. *Nat Protoc* **11**, 2301-2319 (2016). doi:10.1038/nprot.2016.136
80. J. J. Almagro Armenteros *et al.*, Detecting sequence signals in targeting peptides using deep learning. *Life Sci Alliance* **2**, (2019). doi:10.26508/lsa.201900429
81. H. Lenz, A. Hein, V. Knoop, Plant organelle RNA editing and its specificity factors: enhancements of analyses and new database features in PREPACT 3.0. *BMC Bioinformatics* **19**, 255 (2018). doi:10.1186/s12859-018-2244-9
82. S. Bentolila, J. Oh, M. R. Hanson, R. Bukowski, Comprehensive high-resolution analysis of the role of an Arabidopsis gene family in RNA editing. *PLoS Genet* **9**, e1003584 (2013). doi:10.1371/journal.pgen.1003584
83. S. Tyanova, J. Cox, Perseus: A bioinformatics platform for integrative analysis of proteomics data in cancer research. *Methods Mol Biol* **1711**, 133-148 (2018). doi:10.1007/978-1-4939-7493-1_7
84. M. E. Ritchie *et al.*, limma powers differential expression analyses for RNA-sequencing and microarray studies. *Nucleic Acids Res* **43**, e47 (2015). doi:10.1093/nar/gkv007
85. C. Hooper *et al.*, Subcellular Localisation database for Arabidopsis proteins version 5. (2022). doi:10.26182/8dht-4017
86. N. Colaert, K. Helsens, L. Martens, J. Vandekerckhove, K. Gevaert, Improved visualization of protein consensus sequences by iceLogo. *Nat Methods* **6**, 786-787 (2009). doi:10.1038/nmeth1109-786
87. D. Szklarczyk *et al.*, The STRING database in 2023: protein-protein association networks and functional enrichment analyses for any sequenced genome of interest. *Nucleic Acids Res* **51**, D638-D646 (2023). doi:10.1093/nar/gkac1000

88. N. T. Doncheva, J. H. Morris, J. Gorodkin, L. J. Jensen, Cytoscape stringApp: network analysis and visualization of proteomics data. *J Proteome Res* **18**, 623-632 (2019). doi:10.1021/acs.jproteome.8b00702
89. P. Shannon *et al.*, Cytoscape: a software environment for integrated models of biomolecular interaction networks. *Genome Res* **13**, 2498-2504 (2003). doi:10.1101/gr.1239303
90. M. Legeay, N. T. Doncheva, J. H. Morris, L. J. Jensen, Visualize omics data on networks with Omics Visualizer, a Cytoscape App. *F1000Res* **9**, 157 (2020). doi:10.12688/f1000research.22280.2
91. A. Candat *et al.*, The ubiquitous distribution of late embryogenesis abundant proteins across cell compartments in *Arabidopsis* offers tailored protection against abiotic stress. *Plant Cell* **26**, 3148-3166 (2014). doi:10.1105/tpc.114.127316

Acknowledgments: The authors are grateful to Ms. S. Nakae, Ms. K. Kaneko, and Ms. F. Sakai in the support unit for Bio-Material Analysis and RIKEN CBS Research Resources Division for technical help with the nucleotide sequencing analyses. We also thank Prof. M. Matsui and Dr. W.D. Ong at RIKEN for providing the *lea7-1* as well as A. Sato (Plant Genomic Network Research Team) for technical support. We would like to thank Paulina Heinkow for technical support with the LC-MS/MS analysis within the MSPUB proteomics unit of the University of Muenster.

Funding: This work was supported by the following grants and funding agencies:

ASPIRE JPMJAP24A3 (MS)

CREST JPMJCR13B4 (MS)

GteX programs of the Japan Science and Technology Agency JPMJGX23B0 (MS) "Epigenome Manipulation Project" and "Global Commons Project" of RIKEN (MS)

The Ministry of Education Culture, Sports and Technology of Japan KAKENHI Grant 19K05960 (MU)

The Deutsche Forschungsgemeinschaft (DFG, German Research Foundation) – INST 211/744-1 FUGG for instrumentation (IF)

Author contributions:

Conceptualization: MU, MS, IF

Methodology: AI, KS, HT, ST, DS, IF

Investigation: FK, MU, JE, JI, JS, TA,

Visualization: FK, JE, MU,

Funding acquisition: MU, MS, IF,

Project administration: MS, IF,

Supervision: MU, MS, DS, IF,

Writing – original draft: FK, MU,

Writing – review & editing: DS, MS, IF with contribution of all authors.

Competing interests: The authors declare that they have no competing interests.

Data and materials availability: Mass spectrometry proteomics data have been deposited at the ProteomeXchange Consortium (https://proteomecentral.proteomexchange.org/ui) via the JPOSTDB partner repository (https://repository.jpostdb.org/) with the identifiers JPST004010 and PXD067353.

Gene identifiers and sequence information can be found in The Arabidopsis Information Resource-TAIR database (www.arabidopsis.org) under the following accession numbers: HDA19 (AT4G38130), HTR4 (AT4G40030), HTR5 (AT4G40040), HTR8 (AT5G10980), LEA7 (AT1G52690), LEA29 (AT3G15670), RAB18 (AT5G66400). Plasmids and seeds are available from M.S. upon reasonable request.

Supplementary Materials

Figs. S1 to S9

Table S1 to S5

Data S1 to S5

Figures

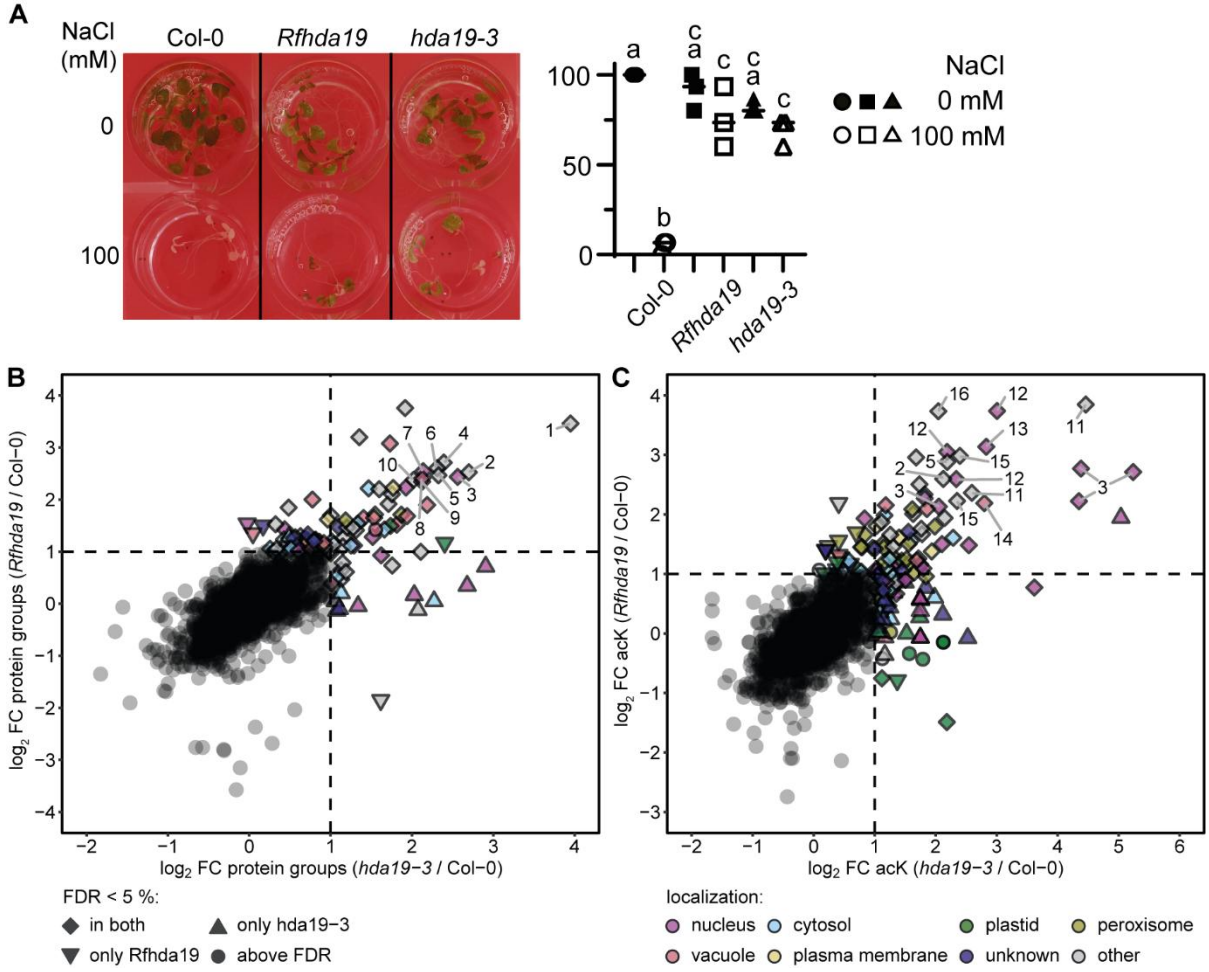

Fig. 1. Identification of lysine-acetylated HDA19 substrates involved in plant stress tolerance. **(A)** *Rfhda19*, a revertant in fertility of the *hda19-7* mutant, exhibited similar tolerance to salinity stress (100 mM NaCl) as *hda19-3*. Multiple comparisons of survival rate were performed using one-way ANOVA, with $P < 0.05$ considered significant (n=3). (**B** - **C**) Scatter plots comparing (**B**) protein groups and (**C**) lysine acetylation (acK) site abundance changes in *hda19-3* vs WT and *Rfhda19* vs WT. The original data can be found in DataS2 and S3. Protein names or symbols of numbered spots are displayed in TableS1.

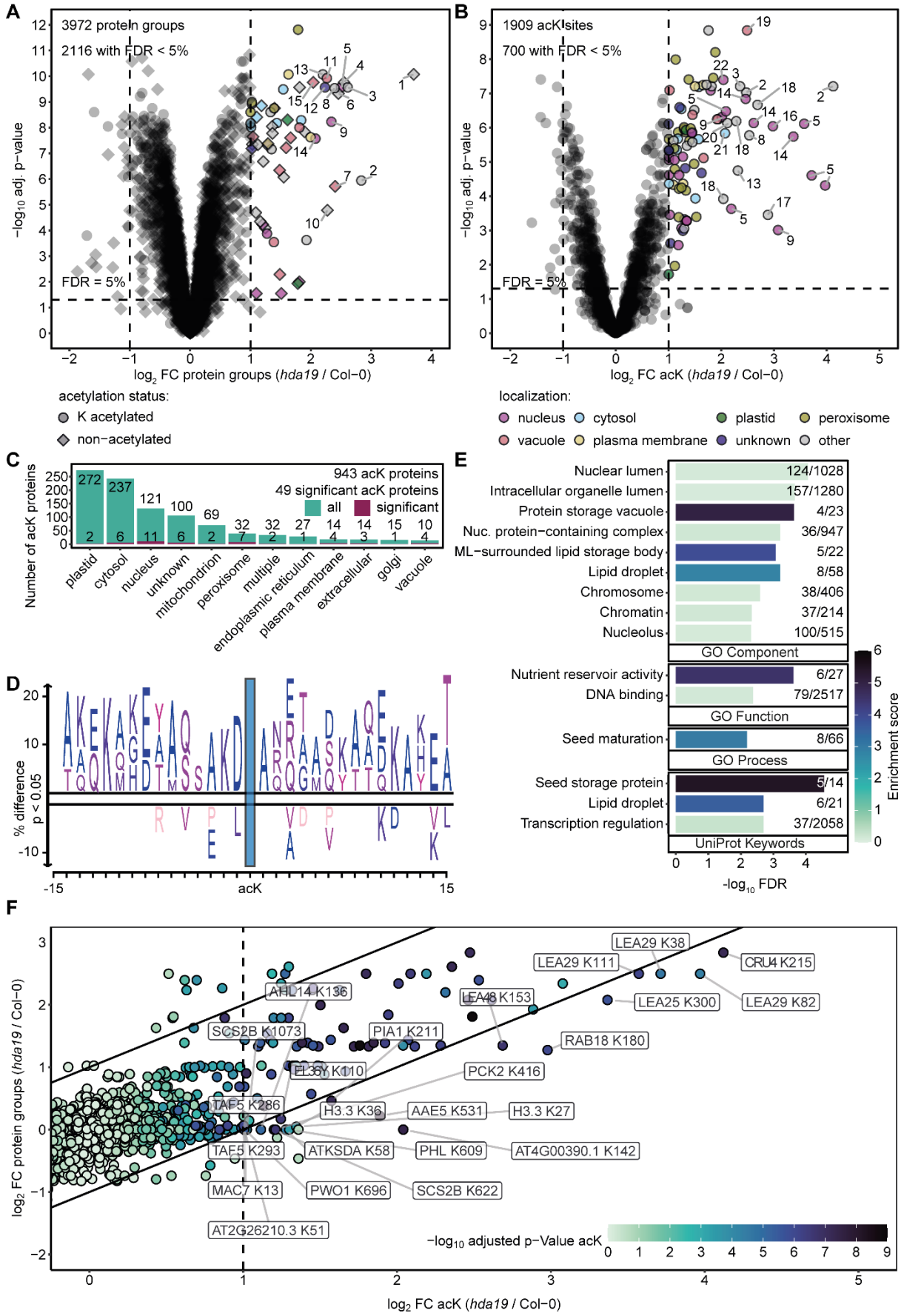
A
3972 protein groups
2116 with FDR < 5%
FDR = 5%
−log10 adj. p−value
log2 FC protein groups (hda19 / Col−0)
acetylation status:
K acetylated
non−acetylated
B
1909 acK sites
700 with FDR < 5%
FDR = 5%
−log10 adj. p−value
log2 FC acK (hda19 / Col−0)
localization:
nucleus
cytosol
plastid
peroxisome
vacuole
plasma membrane
unknown
other
C
943 acK proteins
49 significant acK proteins
all
significant
Number of acK proteins
plastid
cytosol
nucleus
unknown
mitochondrion
peroxisome
multiple
endoplasmic reticulum
plasma membrane
extracellular
golgi
vacuole
D
% difference
p < 0.05
acK
E
Nuclear lumen 124/1028
Intracellular organelle lumen 157/1280
Protein storage vacuole 4/23
Nuc. protein−containing complex 36/947
ML−surrounded lipid storage body 5/22
Lipid droplet 8/58
Chromosome 38/406
Chromatin 37/214
Nucleolus 100/515
GO Component
Nutrient reservoir activity 6/27
DNA binding 79/2517
GO Function
Seed maturation 8/66
GO Process
Seed storage protein 5/14
Lipid droplet 6/21
Transcription regulation 37/2058
UniProt Keywords
-log10 FDR
Enrichment score
F
LEA29 K38
LEA29 K111
CRU4 K215
AHL14 K136
LEA48 K153
LEA25 K300
LEA29 K82
SCS2B K1073
PIA1 K211
RAB18 K180
EL36Y K110
PCK2 K416
TAF5 K286
H3.3 K36
AAE5 K531
H3.3 K27
TAF5 K293
ATKSDA K58
PHL K609
AT4G00390.1 K142
MAC7 K13
PWO1 K696
SCS2B K622
AT2G26210.3 K51
−log10 adjusted p−Value acK
log2 FC protein groups (hda19 / Col−0)
log2 FC acK (hda19 / Col−0)

794

Fig. 2. Identification of lysine-acetylated HDA19 substrates involved in plant stress tolerance. (**A** - **B**) Volcano plots showing (**A**) protein groups and (**B**) lysine acetylation (acK) site $\log_2$ fold abundance changes in *hda19-3* compared to Col-0 WT, along with -$\log_{10}$(adjusted p-values) from *limma* analysis (*84*). The p-values were adjusted using a Benjamini-Hochberg correction. Data from *hda19-3*, *Rfhda19* and WT were processed and analysed as one *hda19* group, and only acK sites and protein groups quantified in at least 6 of 8 biological replicates were included in the analysis. Log_2 fold changes (FC) of +/- 1 and false discovery rates (FDR) of < 5 % are indicated by dashed lines. Significantly altered proteins and acK sites ($\log_2$ FC > 1, FDR < 5 %) are colored according to their SUBA5 localization (*85*). AcK sites and proteins with a $\log_2$ FC > 2 are numbered. Protein numbers with symbols or identifiers from 1 to 22: 1. AT2G05580, 2. CRU4, 3. CRU3, 4. PAP85, 5. LEA29, 6. AT4G36700, 7. LEA18, 8. CRU1, 9. LEA7, 10. CRU2, 11. OLEO2, 12. OLEO4, 13. LEA30, 14. LEA25, 15. CLO1, 16. RAB18, 17. SESA1, 18. LEA48, 19. OLEO1, 20. LEA42, 21. LEA36, 22. AT4G00390. The original data is available in DataS4. (**C**) Subcellular localization of all quantified acetylated proteins (green), and those which are significantly regulated in *hda19* vs WT (purple) with a $\log_2$ fold-change (FC) acK > 1, FDR < 0.05. (**D**) Sequence logo of significantly upregulated acK sites in *hda19* ($\log_2$ FC > 1, FDR < 0.05). The blue box indicates the position of the acetylated lysine residue. (**E**) Functional enrichment analysis of all quantified acetylated proteins in *hda19* vs WT. The bars represent the -$\log_{10}$(FDR) for each term. The color of each bar corresponds to the enrichment score for each term, calculated by STRING. The numbers adjacent to the bars indicate the number of proteins found and the total number for each term. The analysis included GO component, GO function, GO process, and UniProt keywords. Only terms showing an increase in abundance are displayed. (**F**) Comparison of protein and acK $\log_2$-fold changes in *hda19* (*hda19-3* + *Rfhda19*). Nineteen proteins exhibited a significant increase in acetylation at 24 acK sites, exceeding their respective protein abundance changes. The lysine (K) positions of the histone sites were adjusted to account for the removal of the initiator methionine. The original data can be found in Data S4.

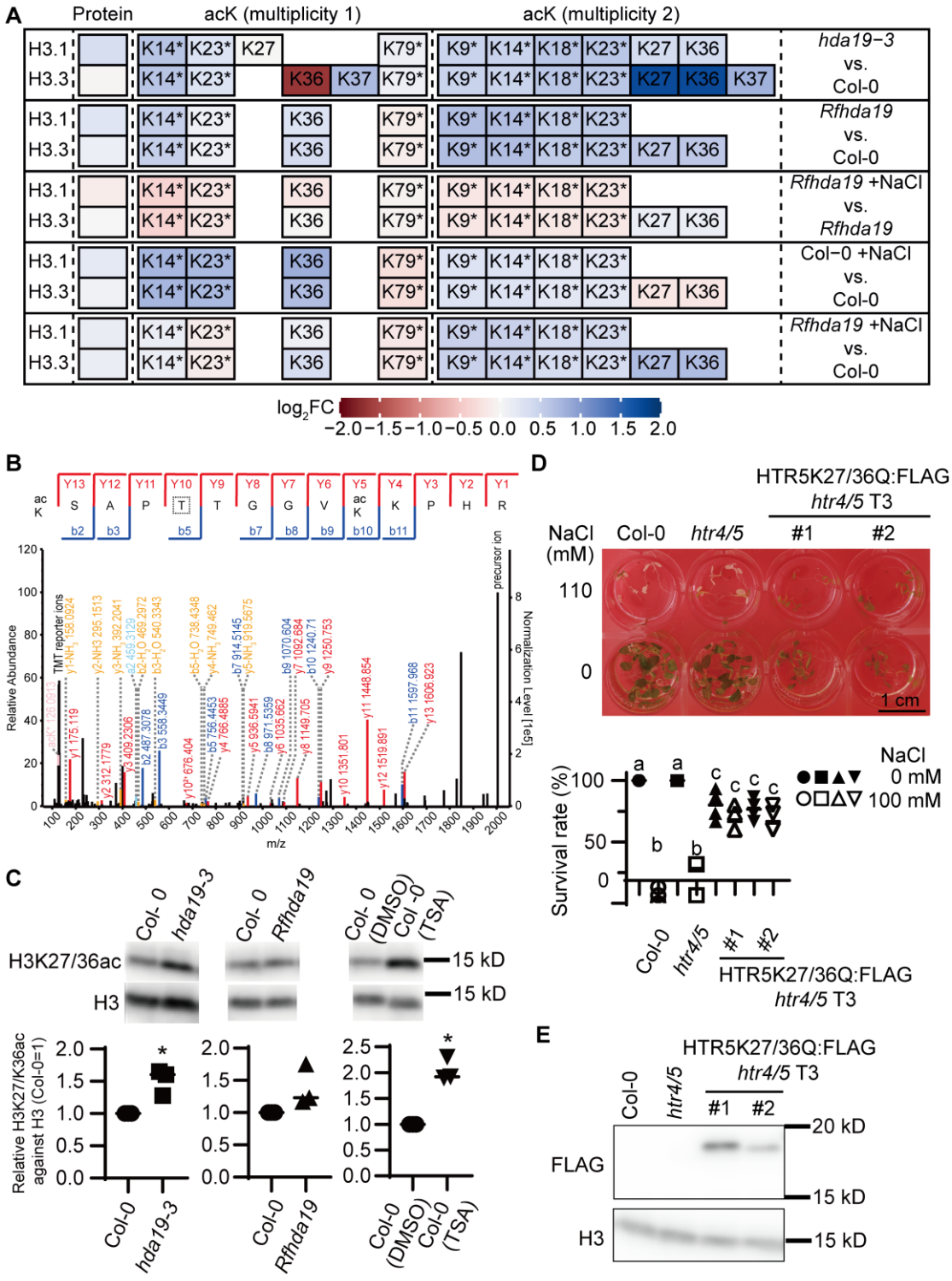

Fig. 3. Requirement of H3.3K27/K36 di-acetylation for enhanced tolerance to salinity stress. (**A**) Protein and acK abundance of the two main histone 3 variants, H3.1 and H3.3, in *hda19-3*, *Rfhda19*, *Rfhda19* + NaCl, and WT + NaCl, were quantified in at least 2 out of 4 biological replicates. Colors indicate the respective $\log_2$ fold change (FC) values. Lysine positions have been adjusted to reflect the cleavage of the initiator methionine. Lysine acetylation (acK) sites are grouped by their respective multiplicity, as determined by MaxQuant. Stars next to the lysine (K) position indicate sites that could belong to both histone variants. (**B**) MS/MS spectra, as processed

by MaxQuant, show an H3.3 peptide carrying K27 and K36 di-acetylation. The amino acid at position 31, which differentiates H3.3 from H3.1, is marked by a dashed box. (**C**) Differences in histone H3 acetylation levels in the *hda19-3*, *Rfhda19*, and plants treated with trichostatin A (TSA) were evaluated. Quantification of relative acetylation levels was perfomed using Student's *t*-test (n=3, $P < 0.05$). (**D**) Expression of FLAG-tagged HTR5K27/K36Q acetylation mimicking variant in *htr4/5* enhanced tolerance to salinity stress (100 mM NaCl). Multiple comparisons of survival rate were performed using one-way ANOVA, with $P < 0.05$ considered significant (n=3). (**E**) Immunoblotting of the FLAG-tagged HTR5K27/K36Q acetylation mimicking variant is shown. The full blot is presented in Supplementary Figure S9.

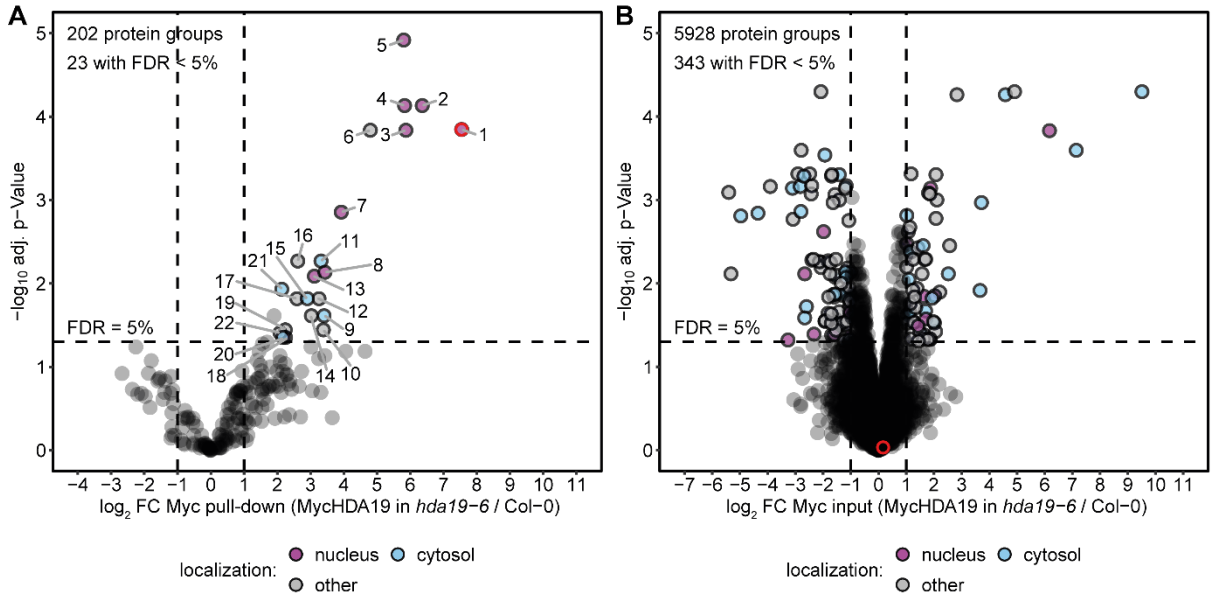

Fig. 4. Identification of HDA19 interacting proteins. Volcano plots showing (A) enriched proteins in Myc pulldown and **(B)** overall protein abundance changes (input) in MycHDA19 (in *hda19-6*) compared to Col-0 WT, along with -$\log_{10}$(adjusted p-values) from *limma* analysis (*84*). The p-values were adjusted with Benjamini-Hochberg correction. Protein groups only quantified in at least 2 of 4 biological replicates were included in the analysis. Log_2 fold changes of +/- 1 and FDR of 5 % are indicated by dashed lines. Significantly enriched proteins ($\log_2$ FC > 1, FDR < 0.05) are colored according to their SUBA5 localization (*85*). Significantly enriched proteins with a $\log_2$ FC > 2 are numbered. Protein numbers with symbols or identifiers from 1 to 22: 1. HDA19, 2. HDC1, 3. ES25Y, 4. MSI1, 5. SNL5, 6. SNL4, 7. SNL6, 8. SNL2, 9. RPL5A, 10. AT5G36790, 11. CCT7, 12. HDIP3, 13. HB1, 14. FdC1, 15. RAN-1, 16. APOK3, 17. ICL, 18. SNL1, 19. CRU2, 20. RPS18C, 21. RPS26e, 22. LACS6. HDA19 is highlighted by a red circle in A and B. The original data can be found in Data S5.

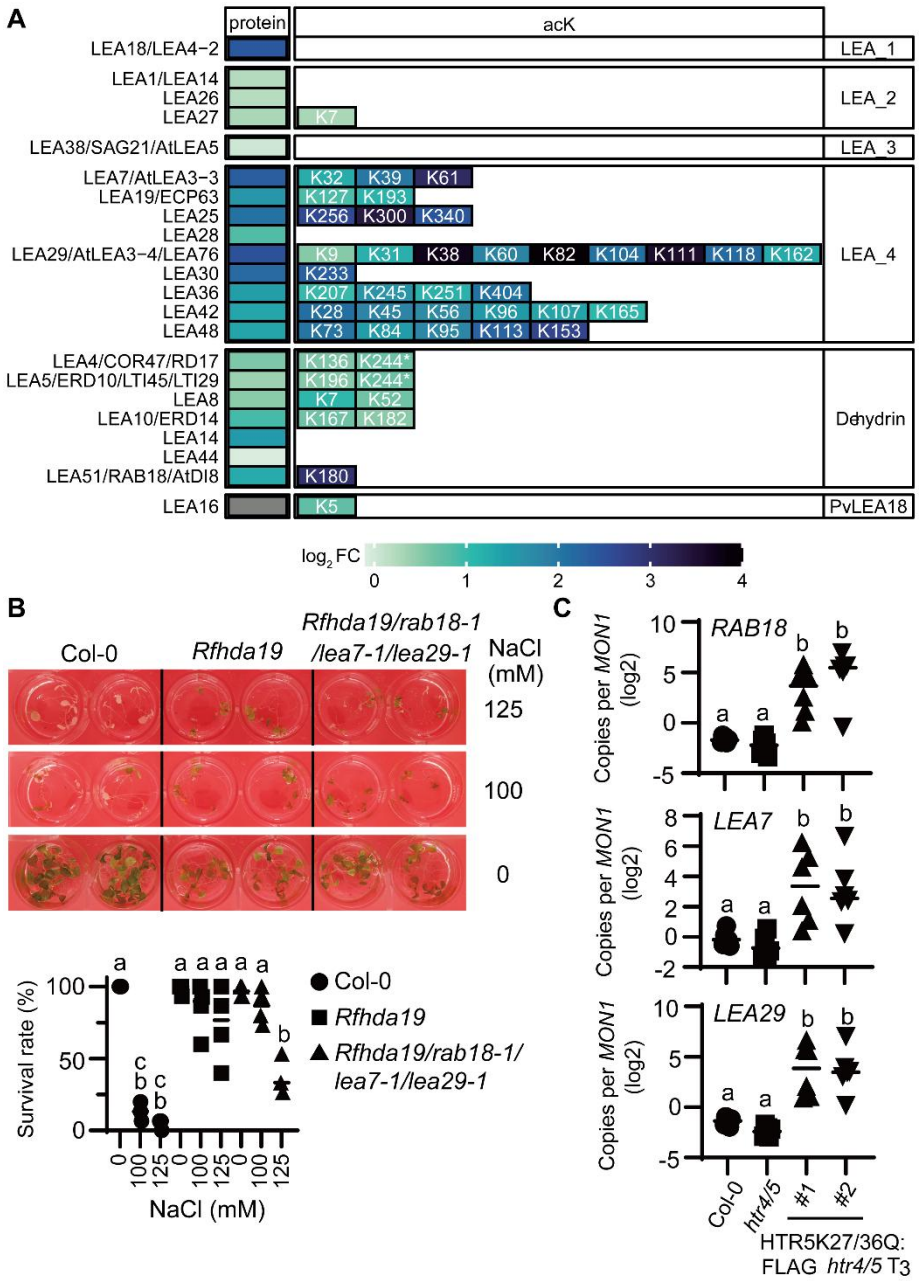

Fig. 5. Identification of essential LEA proteins for enhancing salinity tolerance in *hda19* mutants. (**A**) Protein abundance and lysine acetylation site (acK) levels of LEA proteins, quantified in at least 6 out of 8 replicates, are shown. The color indicates the $\log_2$ fold change (FC) of *hda19* versus WT Col-0. Stars next to the K position indicate sites that could belong to both LEA variants. (**B**) Deficiencies in three *LEA* genes (*RAB18*/*LEA7*/*LEA29*) decreased tolerance to salinity stress in *Rfhda19* mutants under high salinity stress conditions (125 mM NaCl). Statistical analysis was performed using a one-way ANOVA, with $P < 0.05$ considered significant (n=4). (**C**) qPCR analysis of the mRNA expression of *LEA* genes in FLAG-tagged fused HTR5K27/K36Q acetylation mimicking plants. The dataset was normalized using the reference gene (*MON1*). Statistical analysis was performed using one-way ANOVA, with $P < 0.05$ considered significant (n=6). Different letters indicate significant differences.

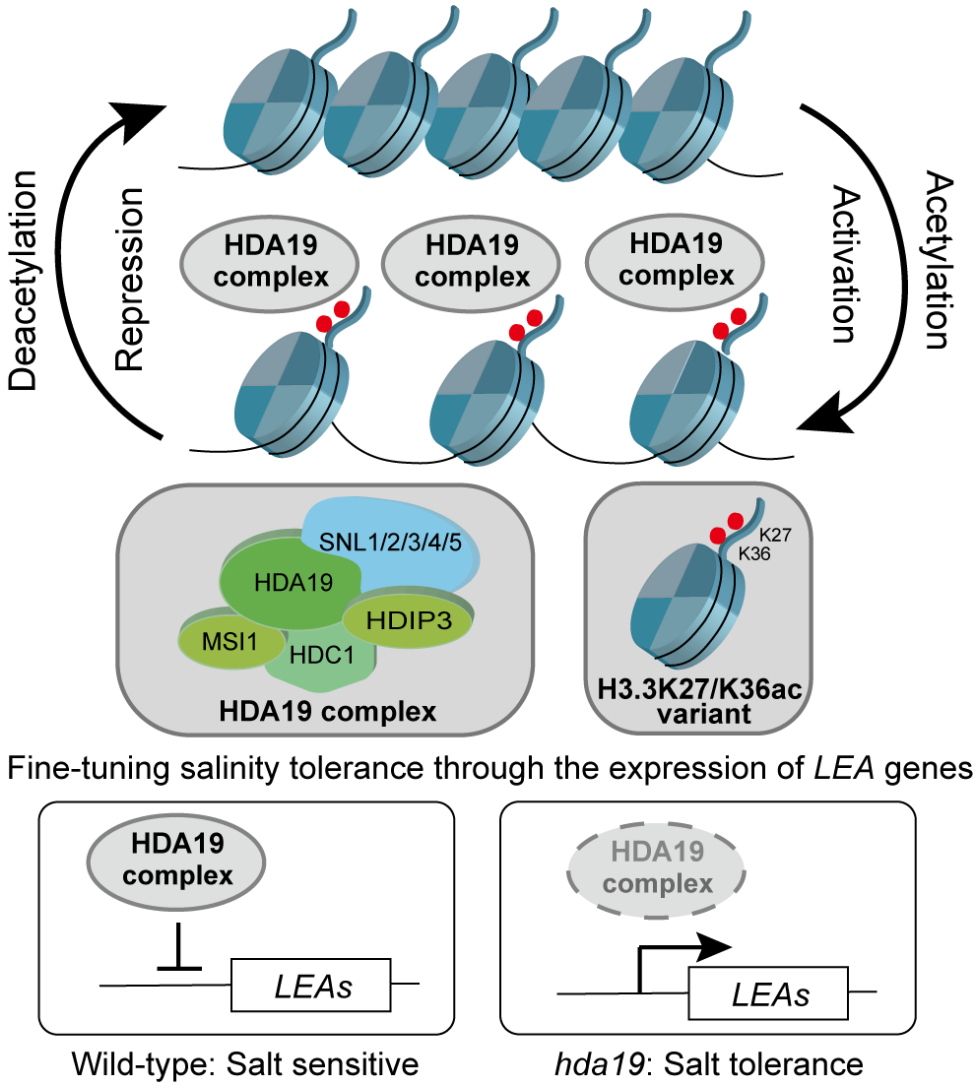

Fig. 6. Schematic representation of a proposed mechanism of the response to salinity stress regulated by HDA19. HDA19 complex regulates the expression of *LEA* genes (e. g. *LEA7/LEA29/RAB18*) through di-acetylation of K27/K36 on histone H3.3.

Supplementary Materials for

HDA19-mediated deacetylation of histone H3.3 lysine 27 and 36 regulates plant sensitivity to salt stress

Florian Kotnik, Minoru Ueda *et al.*

*Corresponding author. Email: motoaki.seki@riken.jp (MS); finkemeier@uni-muenster.de (IF)

This PDF file includes:

Figs. S1 to S9
Tables S1 to S5

Other Supplementary Materials for this manuscript include the following:
Data S1 to S5

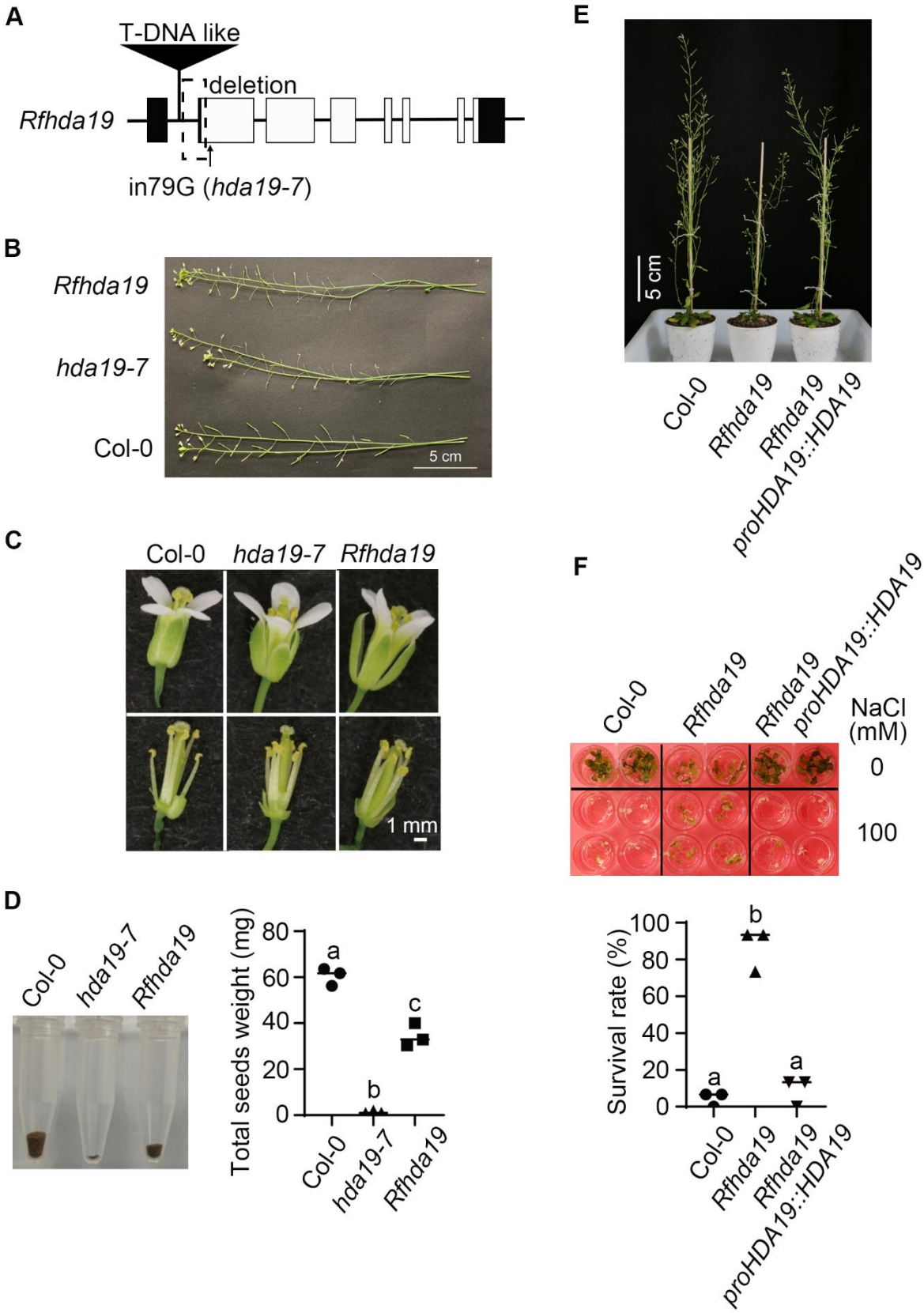
A
T-DNA like
deletion
Rfhda19
in79G (hda19-7)
B
Rfhda19
hda19-7
Col-0
5 cm
C
Col-0
hda19-7
Rfhda19
1 mm
D
Col-0
hda19-7
Rfhda19
Total seeds weight (mg)
80
60
40
20
0
a
b
c
Col-0
hda19-7
Rfhda19
E
5 cm
Col-0
Rfhda19
Rfhda19
proHDA19::HDA19
F
Col-0
Rfhda19
Rfhda19
proHDA19::HDA19
NaCl
(mM)
0
100
Survival rate (%)
100
80
60
40
20
0
a
b
a
Col-0
Rfhda19
Rfhda19
proHDA19::HDA19

Fig. S1.

Characterization of *Rfhda19* (Reverted fertility in *hda19*). (**A**) Genome rearrangements around the *HDA19* locus in *hda19-7*. (**B**) Morphological phenotype of the siliques of the main stem in *Rfhda19*. (**C**) Morphological phenotype of stamen and pistil in *Rfhda19* at stage14, as defined Smyth et al 1990 (*66*). (**D**) Comparison of seed numbers harvested from three individual plants of *Rfhda1*9. (**E**) Complementation of *Rfhda1*9 with a HDA19 genomic fragment. (**F**) Loss of salinity stress tolerance upon complementation of HDA19 in *Rfhda1*9. Statistical analyses in D and F were performed using a one-way ANOVA test ($P < 0.05$, n=3). Different letters indicate significant differences.

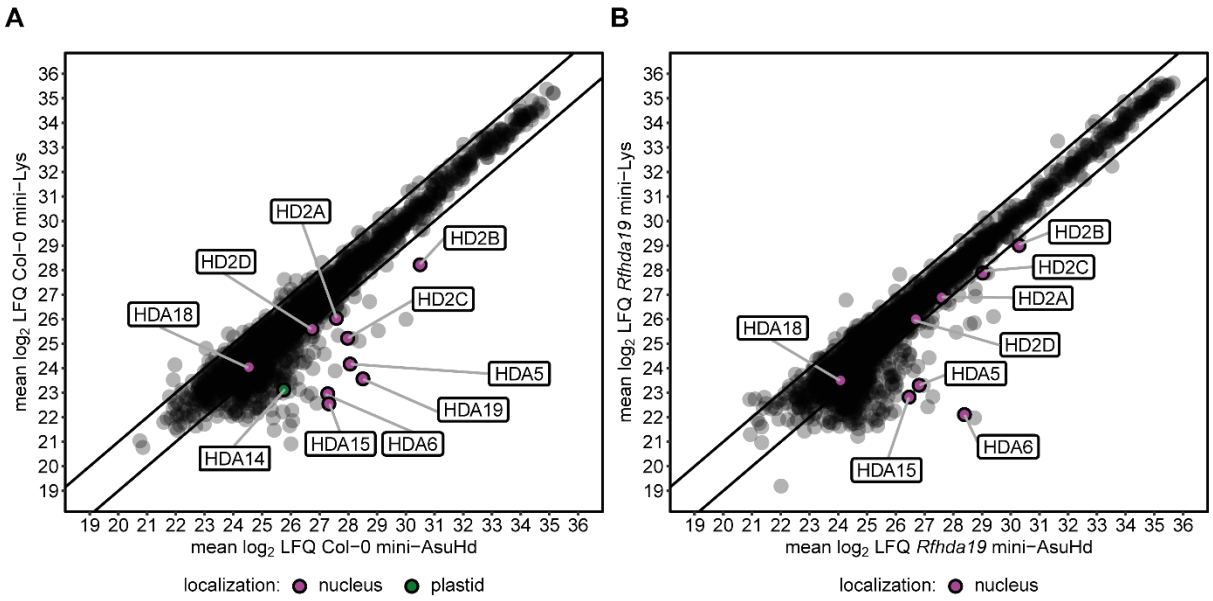

Fig. S2.

***Rfhda19* is a lacking an active HDA19 enzyme.** (**A** - **B**) Scatter plots comparing mean $\log_2$ LFQ values of mini-AsuHd and mini-Lys pull-downs in (**A**) Col-0 WT and (**B**) *Rfhda19* (n = 2). All quantified HDACs are labeled and colored according to their subcellular localization based on SUBA5 (*85*) The original data can be found in DataS1.

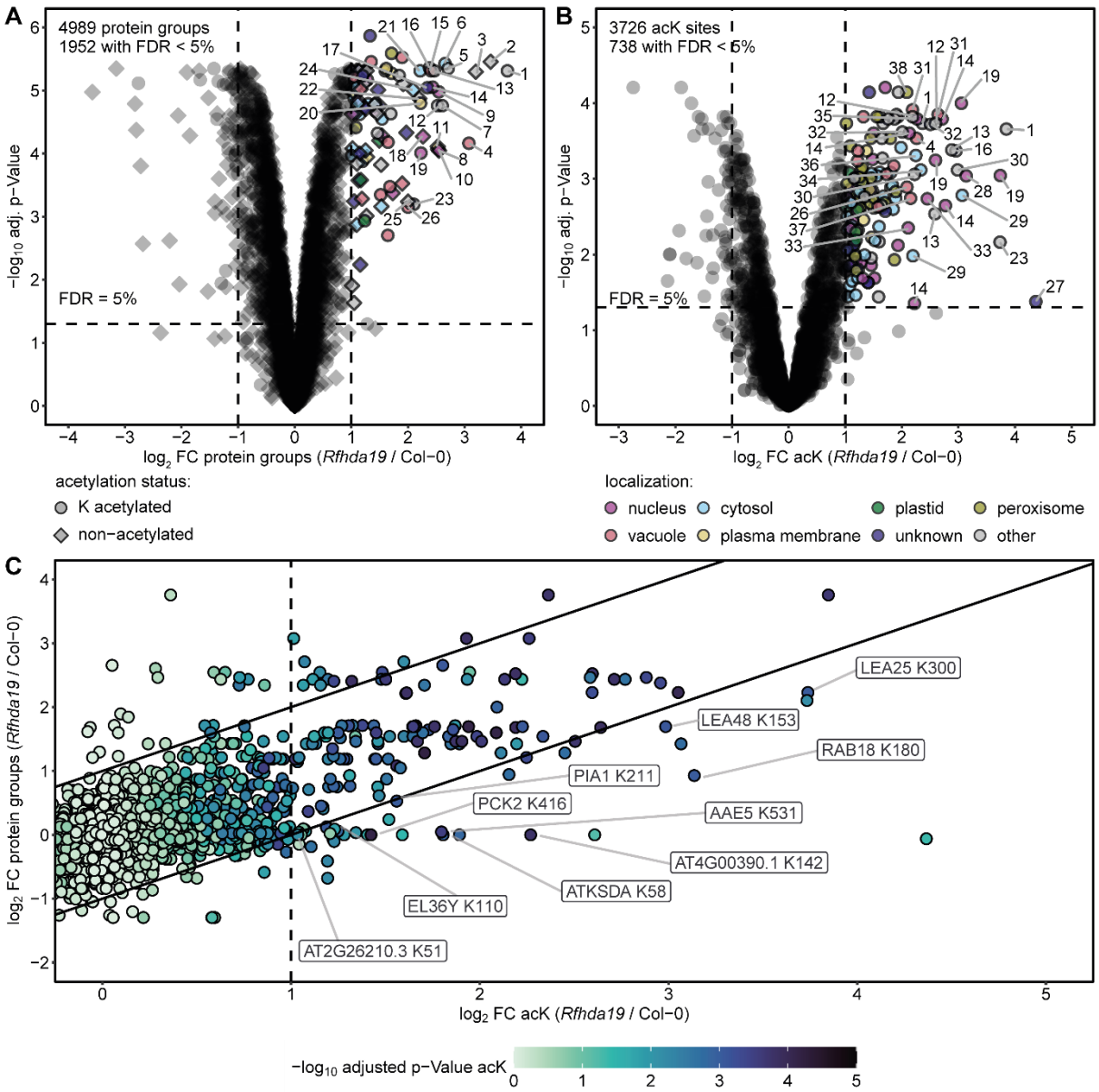

Fig. S3.

Quantitative proteome and lysine acetylome of *Rfhda19* compared to Col-0 WT. (**A** - **B**) Volcano plots showing (**A**) protein groups and (**B**) lysine acetylation (acK) site $\log_2$ fold abundance changes in *Rfhda19* compared to Col-0 WT, along with -$\log_{10}$(adjusted p-values) from *limma* analysis (*84*). The p-values were adjusted using a Benjamini-Hochberg correction. Only acK sites and protein groups quantified in at least 2-4 biological replicates were included in the analysis. Log_2 fold changes (FC) of +/- 1 and false discovery rates (FDR) of < 5 % are indicated by dashed lines. Significantly altered proteins and acK sites ($\log_2$ FC > 1, FDR < 5 %) are colored according to their SUBA5 localization (*85*). AcK sites and proteins with a $\log_2$ FC > 2 are numbered. Protein numbers with symbols or identifiers from 1 to 38: 1. CRU4, 2. AT2G05580, 3. CRU2, 4. LEA18, 5. PAP85, 6. TASTY, 7. AT4G36700, 8. RD29B, 9. LEA7, 10. AT2G18540, 11. AT3G20730, 12. CRU3, 13. CRU1, 14. LEA29, 15. OELO2, 16. LEA30, 17. OELO4, 18.

AT2G29065, 19. LEA25, 20. ATS3, 21. PER1, 22. AT2G28490, 23. SESA1, 24. ATXIE1, 25. AT5G35660, 26. SESA3, 27. DRP1A, 28. RAB18, 29. ECP63, 30. LEA48, 31. OLEO1, 32. LEA42, 33. SLDP1, 34. LEA36, 35. AT4G00390, 36. PCK1, 37. OLEO3, 38. mLS. (**C**) Scatter plot of $\log_2$ acK FC against $\log_2$ protein FC of *Rfhda19* vs WT. Only acK sites with a $\log_2$ FC > 0 are shown. Colors indicate the $-\log_{10}$(adjusted p-value) of acK site changes. $\log_2$ acK FC > 1 is indicated by a dashed line. Diagonal lines (slope = 1, intercepts = +/- 1) represent an absolute fold change difference of 1 between acK sites and proteins. Only proteins/acK sites which are also labeled in Fig. 1C are labeled here. The original data can be found in DataS2.

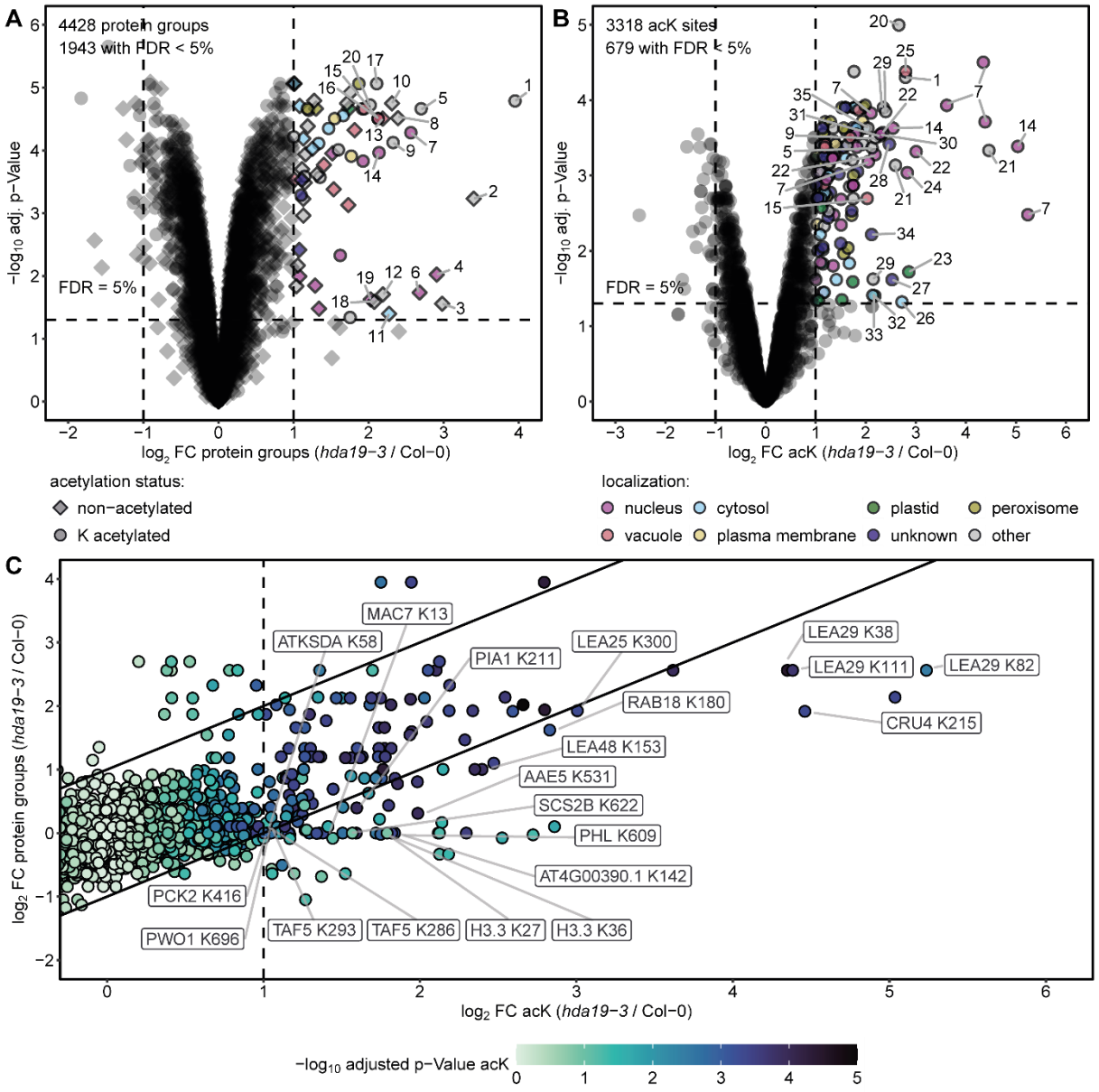

Fig. S4.

Quantitative proteome and lysine acetylome of *hda19-3* compared to Col-0 WT. (**A** - **B**) Volcano plots showing (**A**) protein groups and (**B**) lysine acetylation (acK) site $\log_2$ fold abundance changes in *hda19-3* compared to Col-0 WT, along with -$\log_{10}$(adjusted p-values) from *limma* analysis (*84*). The p-values were adjusted using a Benjamini-Hochberg correction. Only acK sites and protein groups quantified in at least 2-4 biological replicates were included in the analysis. Log_2 fold changes (FC) of +/- 1 and false discovery rates (FDR) of < 5 % are indicated by dashed lines. Significantly altered proteins and acK sites ($\log_2$ FC > 1, FDR < 5 %) are colored according to their SUBA5 localization (*85*). AcK sites and proteins with a $\log_2$ FC > 2 are numbered. Protein numbers with symbols or identifiers from 1 to 35:

1. AT2G05580, 2. TRP3, 3. GRP3, 4. GRP2B, 5. CRU3, 6. GRP2, 7. LEA29, 8. PAP85, 9. CRU1, 10. AT4G36700, 11. RPS13, 12. AT1G47540, 13. CLO1, 14. LEA7, 15. OLEO2, 16. OLEO4, 17. SBTI1.1, 18. HEL, 19. PUX7, 20. LEA30, 21. CRU4, 22. LEA25, 23. NIR, 24. RAB18, 25. OLEO1, 26. AXS2, 27. LOS1, 28. ChlADR, 29. LEA48, 30. TAF14B, 31. PER1, 32. RBCS1A, 33. LOS2, 34. TAF5, 35. SESA1. (**C**) Scatter plot of log2 acK FC against log2 protein FC of *hda19-3* vs WT. Only acK sites with a log2 FC > 0 are shown. Colors indicate the -log10(adjusted p-value) of acK site changes. log2 acK FC > 1 is indicated by a dashed line. Diagonal lines (slope = 1, intercepts = +/- 1) represent an absolute fold change difference of 1 between acK sites and proteins. Only proteins/acK sites which are also labeled in Fig. 1C are labeled here. The original data can be found in DataS2.

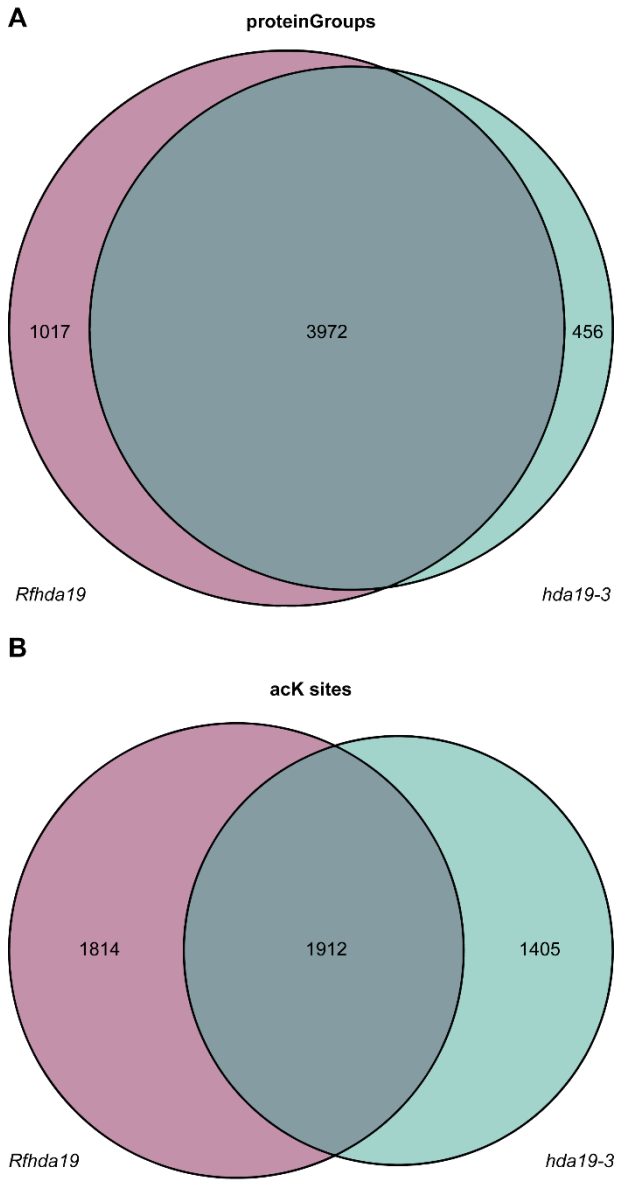

Fig. S5.

Venn diagrams showing overlap of proteomes between *Rfhda19* and *hda19-3*. Overlap of (**A**) protein groups and (**B**) lysine acetylation (acK) sites between *Rfhda19* and *hda19-3*. Proteins and acK sites quantified in at least two out of four biological replicates were used. The original data can be found in DataS2 and DataS3.

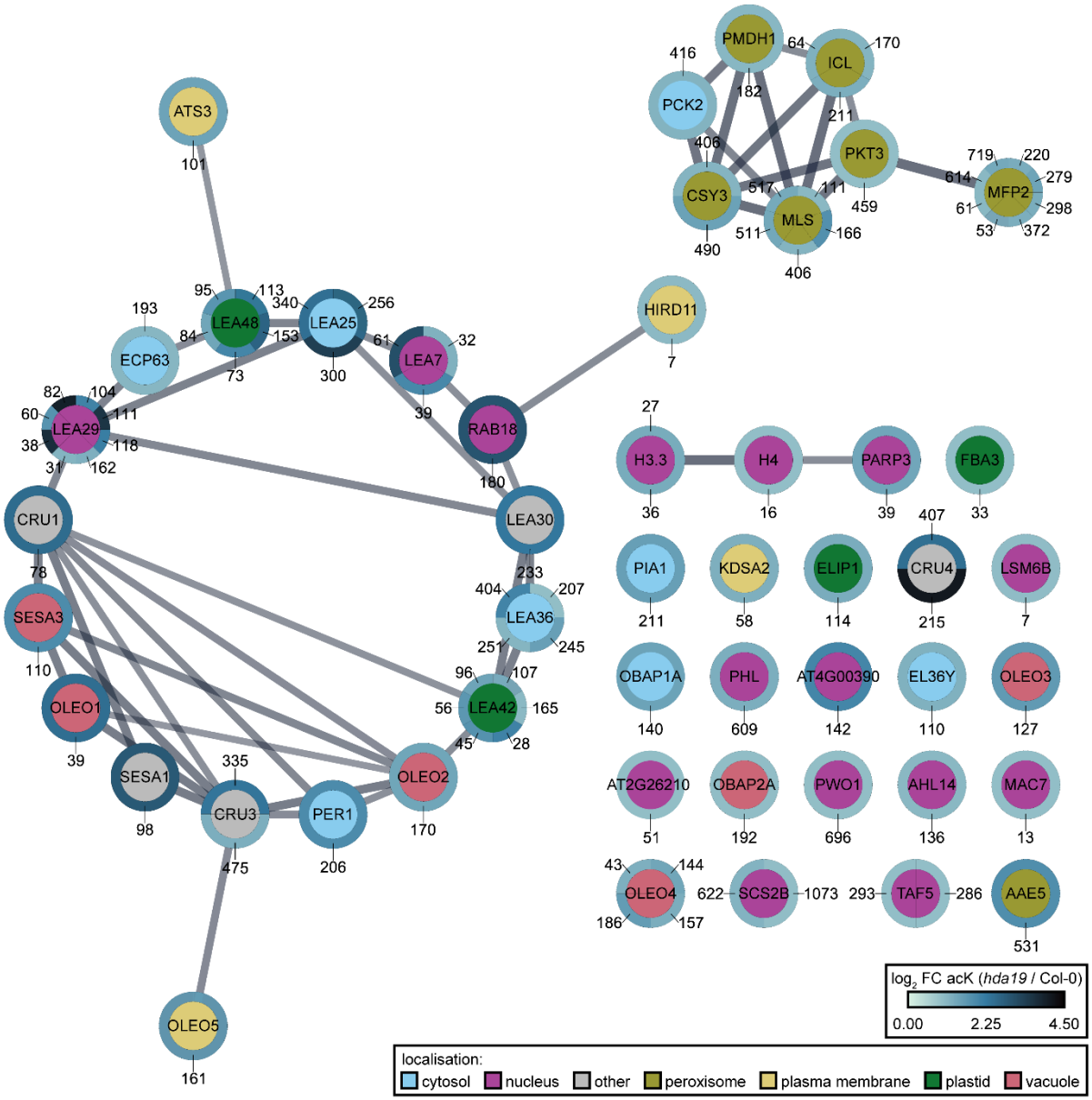

Fig. S6.

STRING network of hyperacetylated proteins in *hda19*. The network was generated using Cytoscape (*88*) and includes hyperacetylated proteins ($\log_2$ FC acK > 1, FDR < 0.05) identified in the combined analysis of *hda19-3* and *Rfhda19*. The outer circle color represents $\log_2$ FC of acK sites according to the color scale, with blue indicating higher values. The position of each acK site is indicated by the outer labels. For histone proteins, lysine positions have been adjusted to reflect their position after removal of the starter methionine. The circle inner color represents subcellular localization, as annotated by SUBA5 (*85*). The localization of LEA proteins was updated based on Candat et al 2014 (*91*). For proteins with unknown localization due to splice forms not present in SUBA5, the localization of the first splice form was assumed. The original data is available in DataS4.

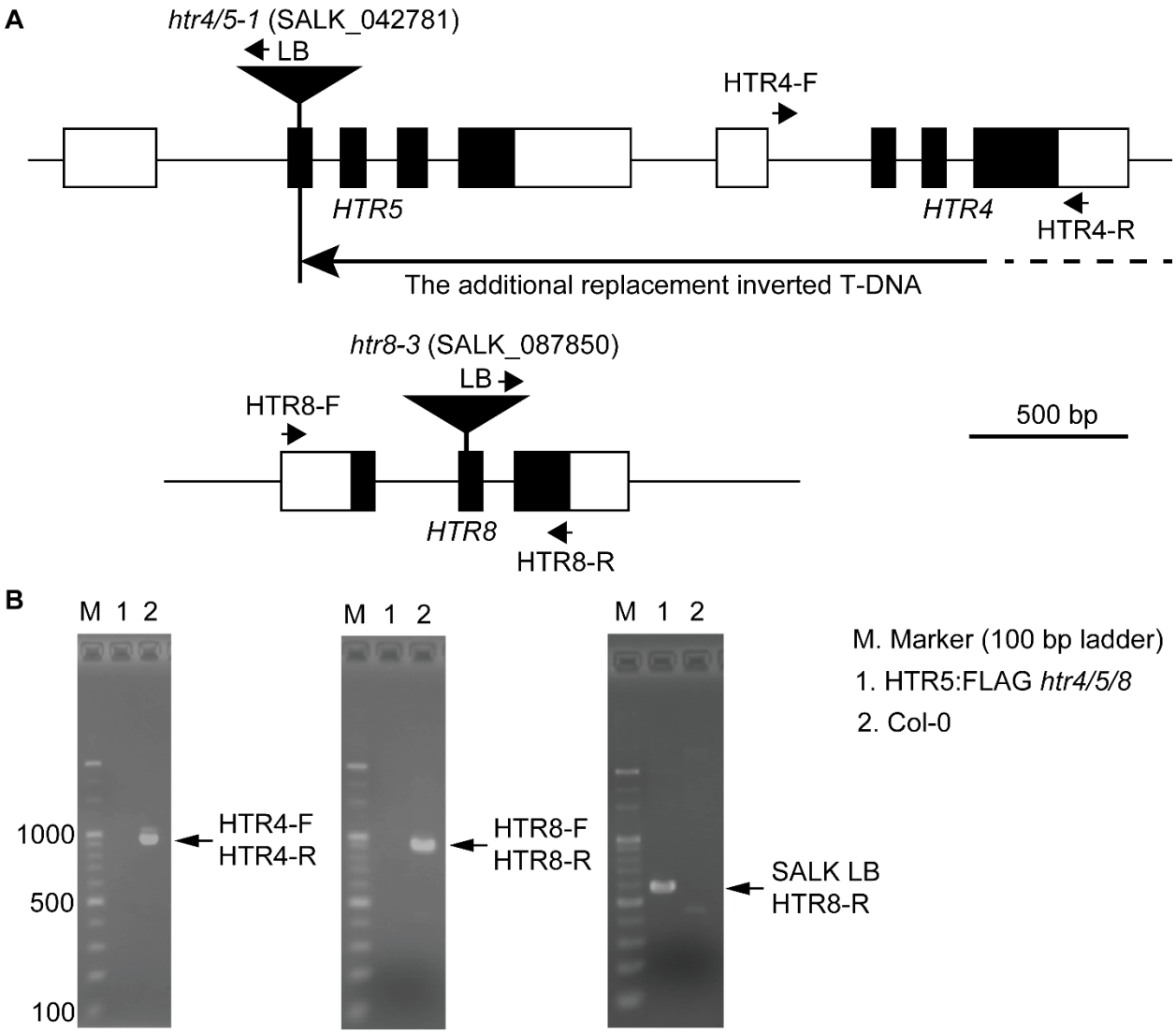

Fig. S7.

Confirmation of *htr4/5/8* triple mutant used to generate a complement line rescued by HTR5:FLAG expression. (**A**) Schematic representation of the *HTR4*, *HTR5*, and *HTR8* gene structures and the T-DNA insertions in *htr4/5-1* (SALK_042781) and *htr8-3* (SALK_087850) according to (*64*). Black boxes, white boxes, and triangles represent exons, untranslated regions, and T-DNA, respectively. Arrows represent primer pairs used for PCRs in B. The information on primer sequences used for B is available from Liu et al 2024 (*64*). (**B**) Gel electrophoresis of PCR products for a T-DNA insertion site in *htr8-3*, and deletion of *HTR4* in *htr4/5-1*.

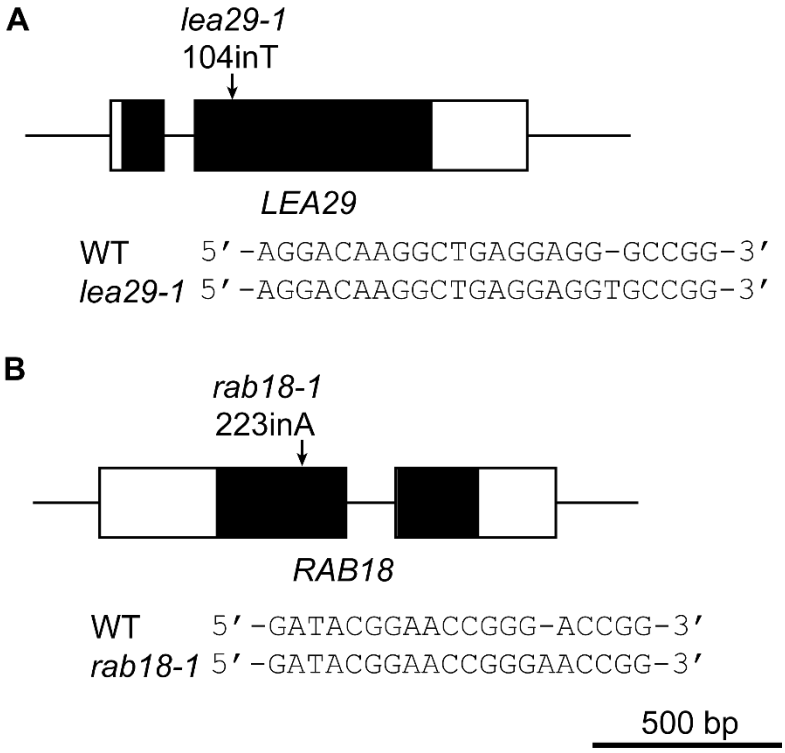

Fig. S8.

Scheme of the *lea29-1* and *rab18-1* mutations. The two mutants *lea29-1* and *rab18-1* are single nucleotide insertion mutants generated by using clustered regularly interspaced short palindromic repeats (CRISPR)/Cas9 system. (**A**) A thymine insertion occurred 104 nt downstream from the LEA29 translational initiation codon. (**B**) An adenine insertion occurred 223nt downstream from the RAB18 translational initiation codon.

Fig. 2C

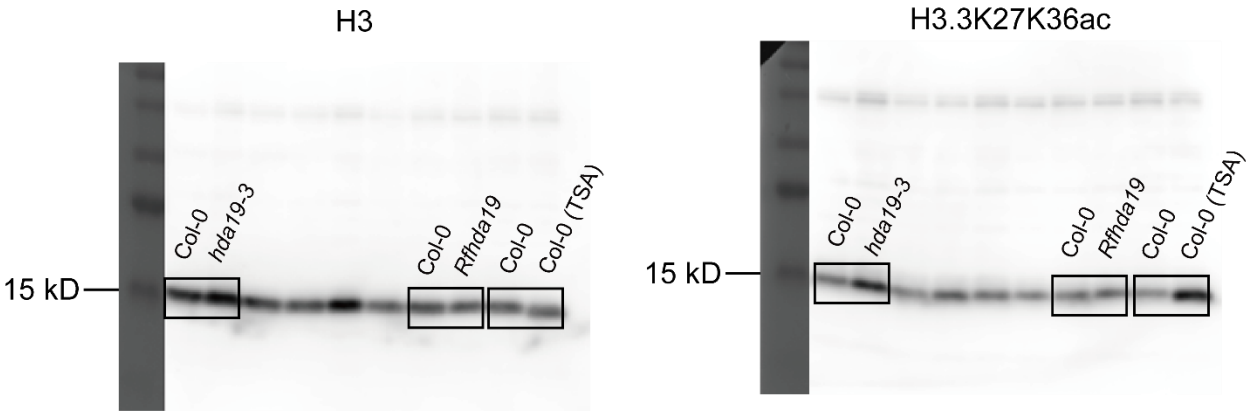

Fig. 2E

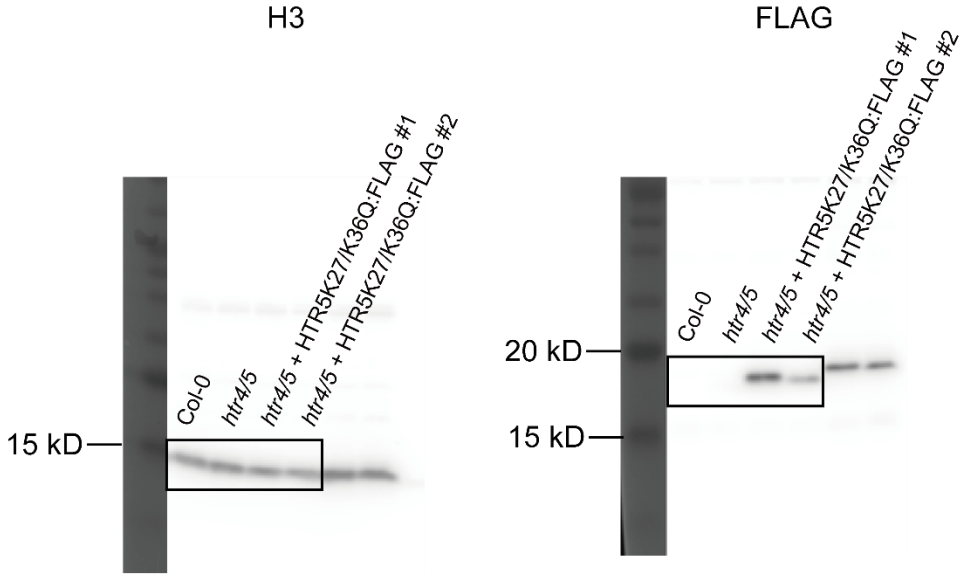

Fig. S9. Full-size images of western blots presented in fig. 2C and 2E.

Table S1.

Identifiers of proteins numbered 1-16 in Fig. 1B and 1C.

number	symbol/identifier	locus
1	AT2G05580	AT2G05580
2	CRU3	AT4G28520
3	LEA29	AT3G15670
4	PAP85	AT3G22640
5	CRU1	AT5G44120
6	AT4G36700	AT4G36700
7	LEA7	AT1G52690
8	OLEO2	AT5G40420
9	OLEO4	AT3G27660
10	LEA30	AT3G17520
11	CRU4	AT1G03890
12	LEA25	AT2G42560
13	RAB18	AT5G66400
14	OLEO1	AT4G25140
15	LEA48	AT5G44310
16	SESA1	AT4G27140

Table S2.

Primers for genome editing.

Target gene	Forward primer	Reverse primer
RAB18	5’-ATTGAAGGATACGGAACCGGGACC-3’	5’-AAACGGTCCCGGTTCCGTATCCTT-3’
LEA29	5’-ATTGGGACAAGGCTGAGGAGGGCC-3’	5’-AAACGGCCCTCCTCAGCCTTGTCC-3’

Table S3

Primers for site-direct mutagenesis. Underline shows a mutated codon.

Mutation site	Forward primer	Reverse primer
HTR5 K27Q	5’-GGCTGCACGTcAGTCTGCACC-3’	5’-GGTGCAGACTgACGTGCAGCC-3’
HTR5 K36Q	5’-TGGAGGAGTCcAGAAGCCCCA-3’	5’-TGGGGCTTCTgGACTCCTCCA-3’
HRT5 full length genomic	5’-CCTTGCCAATCCATATCTGA-3’	5’-GGGGATGATTGAAGTAGTGG-3’

Table S4

Primers for quantitative RT-PCR.

Gene	Forward primer	Reverse primer
LEA7	5'-CACAGAGGAAGTGAAGAGGATAAA-3'	5'-CAACAACAAGGATCGGCATAAC-3'
LEA29	5'-GACTTATCAGAGGAAGTGATGAGAA-3'	5'-CAGCTGAACCACAACCATAAAG-3'
RAB18	5'-AGAAGAACATGGCGTCTTACC-3'	5'-CGGATTTCCGTACTCGTCATAC-3'
MON1	5'-CCGATGACTTGCTTCTACTCTC-3'	5'-CTGAGCGTTGTATCTTGGTAGG-3'

Table S5.

LC-MS/MS data acquisition settings used in this study.

Parameter	Proteome *Rfhda19* vs. Wt *hda19-3* vs Wt Acetylome *Rfhda19* vs. Wt	Acetylome *Rfhda19* vs. Wt (unfractionated) *hda19-3* vs. Wt	HDAC pull-down	Myc pull-down	Input Myc pull-down
Orbitrap resolution for MS^1 scans	120,000	120,000	120,000	120,000	60,000
Scan range (m/z)	380-1500	380-1500	280-1500	300-1759	300-1759
max. injection time	100 ms	100 ms	100 ms	55 ms	55 ms
automatic gain control target MS^1	300%	300%	300%	3e6	3e6
Allowed precursor charge state for fragmentation	2-6	2-6	2-6	2-5	2-5
Number of dependent scans	20	20	20	12	15
Exclusion duration for dynamic exclusion	40 sec	40 sec	40 sec	30 sec	30 sec
Mass tolerance for dynamic exclusion	±10 ppm	±10 ppm	±10 ppm	±10 ppm	±10 ppm
Isolation window (m/z) (no offset)	0.7	0.7	1.6	1.2	1.3
Normalized collision energy	36%	36%	30%	25%	25%
Orbitrap resolution for MS^2 scans	30,000	30,000	15,000	15,000	15,000

Fixed first mass (m/z)	100	100	100	100	100
Max injection time	86 ms	150 ms	150 ms	150 ms	55 ms
Automatic gain control target MS^2	50%	5%	5%	5e4	1e5

Data S1. (separate file)

Quantitative LC-MS/MS analysis of pull-downs using mini-AsuHd HDAC traps and mini-Lys control probes.

Data S2. (separate file)

MS2-based quantitative analysis of the *Rfhda19* vs WT proteome (A) and lysine acetylome (B).

Data S3. (separate file)

MS2-based quantitative analysis of the *hda19-3* vs WT proteome (A) and lysine acetylome (B).

Data S4. (separate file)

Combined analysis of the *hda19* vs WT (A) proteome and (B) lysine acetylome.

Data S5. (separate file)

Quantitative LC-MS/MS analysis of (A) MycHDA19 pull-down and (B) input proteome.